



University of
Stavanger

Faculty of Science and Technology

MASTER'S THESIS

Study program/Specialization: Petroleum Engineering/ Natural Gas Engineering	Spring semester, 2017 Open
Writer: Ellen Lode Tønnessen (Writer's signature)
Faculty supervisor: Rune W. Time Co-supervisor: Hermonja A. Rabenjafimanantsoa	
Thesis title: Measurement of gas fraction in gas-liquid flows using a buoyancy sensor	
Credits (ECTS): 30	
Key words: Gas fractions Buoyancy Multiphase flow Pressure	Pages: 70 + enclosure: 18 Stavanger, 13.07.2017 Date/year

Acknowledgment

This Master This Master thesis was accomplished at the Department of Petroleum Engineering, Faculty of Science and Technology at the University of Stavanger (UiS) spring 2017. The thesis has theory as the point of departure and shows how theory can be applied to develop a new method through experiments, which I performed in the department's Multiphase Laboratory.

I want to thank my supervisors for the opportunity to write an experimental thesis that I found very interesting. Thanks to my head supervisor Professor Rune W. Time for valuable inputs, good comments and positive feedback. Thanks to co-supervisor PhD student Milad Khatibi for all his help.

I also want to thank Senior Engineer Hermonja A. Rabenja Manantsoa for valuable assistance in the laboratory and Laboratory Assistant Kim Andre Nesse Vorland for helping me when technical problems occurred. They made it possible for me to complete my experiments in due time. Thanks to Tor Tønnessen and Marianne Lode Tønnessen for helping with proof-reading and feedback.

Abstract

In this thesis, an innovative new method for measuring in-situ gas fraction in vertical flowing pipes is proposed as an alternative to using differential pressure. The new method has been tested by developing an experimental test setup, and running experiments at the University of Stavanger's Multiphase Laboratory. Key elements in the setup is a stationary pendulum immersed into a pipe filled with water and gas, and connected to a force sensor. By measuring the apparent weight of the pendulum, theory of buoyancy is used to calculate the gas fraction in the pipe. The gas fraction inside the pipe are controlled by using a flow meter to inject gas from the bottom of the pipe. The in-situ gas fraction calculated with the new method are verified by comparing it with readings of the liquid level of fluid inside the pipe and by using a differential pressure gauge simultaneously in the experimental setup.

In order to find an adequate experimental setup, a lot of trial and error in the experimental setup were necessary. During the trial and error period the design and density of the pendulum, the accuracy of the force sensor, the viscosity of the fluid, and type of gas injector were noticed to be of great importance to prevent movement of the pendulum and to get reliable results.

The results from the experiments showed a clear connection between the apparent weight of the pendulum measured by the force sensor and the expected buoyancy of the pendulum for different gas fractions. A comparison with the results from the use of the already existing differential pressure method showed that as the differential pressure, the apparent weight of the pendulum is also affected by pressure gradients. Including to depending on the pressure in the fluid, the apparent weight of the pendulum, was also found to be dependent on a linear force which is most likely caused by viscous forces.

These experimental results are promising. However, further research and development are needed before the new method can be tested out on in an industrial setting.

Table of contents

Acknowledgment	ii
Abstract	iii
Table of contents	iv
List of figures	vi
1. Introduction.....	8
1.1 Background and objective	8
1.2 Experiments and project work	8
1.3 Structure and content	9
2. Theory	11
2.1 Buoyancy (Archimedes principle).....	11
2.2 Dynamic systems of a pendulum.....	14
2.3 Two phase flow regimes in upward gas-liquid flow in vertical pipes.....	15
2.4 Pressure gradients	17
3. Experimental Part.....	19
3.1 Feasibility test.....	19
3.1.1 Setup feasibility test	19
3.1.2 Feasibility test method	21
3.2 Main experimental setup	22
3.2.1 Flow loop with pressure gauges	24
3.2.2 Flow meter, gas pipes and pressure gauges.....	25
3.2.3 Force sensor and pendulum.....	25
3.3 Software.....	25
3.3.1 Modification of the LabVIEW program.....	26
3.3.2 Changes in the LabVIEW programs due to technical problems	27
3.3.3 Calibration the differential pressure gauge	28
3.4 Running the experiments	28
4. Analytical methods	29
4.1 Finding the volume of the bob.....	29
4.2 Experimental data processing.....	29
4.3 Differential pressure	30
4.4 Determining the gas fraction in the system	32

4.4.1	The differential pressure method.....	32
4.4.2	The liquid level method.....	33
4.5	Calculating the expected apparent weight of the pendulum by using Archimedes principle	36
5.	Results and discussion	38
5.1	Modifications in experimental setup	38
5.1.1	Feasibility experiments	38
5.1.2	Converting from the feasibility test to the main experiment setup	45
5.1.3	Bubbles attaching to the bob	50
5.2	Analysis of the results from the final experiments	51
5.2.1	Apparent Weight of the Pendulum.....	52
5.2.2	Differential Pressure Measurement.....	53
5.2.3	Gas Fractions from the Liquid Level Method	54
5.2.4	Comparison between the Liquid Level - and the Differential Pressure Method for finding gas fractions	55
5.2.5	Gas fractions at different injection rates	57
5.2.6	Can a buoyancy sensor be used to measure gas fraction in a gas-liquid flow?..	58
6.	Conclusion	68
7.	Future studies	70
	References (EndNote)	71
	Appendices	72
A.	Specifications.....	72
A.1	PASCO Measurement Equipment	72
A.2	Mark-10 Measurement Equipment	73
A.3	Alicat flow meter	74
B.	MATLAB.....	75
C	Figures.....	81
Calibration of the Differential Pressure Gauge.....		85
Nomenclature		87
Abbreviations.....		87
Greek letters.....		87
Roman Letters.....		87

List of figures

Figure 1 Forces acting on a submerged object	13
Figure 2 Difference between a) the true weight of an object and b) the apparent weight of an object	14
Figure 3 Forces acting on a pendulum	15
Figure 4 Flow regimes in vertical pipes for two-phase flow.[2]	16
Figure 5 Flow regime map in vertical pipes for two-phase flow.[2]	16
Figure 6 Feasibility test set up for a) PASCO force sensor and b) Mark-10 force sensor	20
Figure 7 Feasibility set up with a) no gas injection B) gas injection	22
Figure 8 Flowchart of the setup with data logging	23
Figure 9 Illustration of the flow loop	24
Figure 10 LabVIEW front panel	26
Figure 11 Differential pressure gauge	30
Figure 12 Estimation of gas expansion in the liquid level method	34
Figure 13 Fishing weight	39
Figure 14 Acrylic glass cylinder	40
Figure 15 The coned Acrylic cylinder	40
Figure 16 Comparison of the change in average weight as a function of gas fraction of the bobs tested in the feasibility experiments.	41
Figure 17 Comparison of the mark-10 force sensor and the PASCO 5N load cell	43
Figure 18 Comparison in average apparent weight of the pendulum for PAC4 solution and water	44
Figure 19 Comparison between the gas bubbles inside a PAC4 solution (left) and in water (right) at a gas fraction of 0.0214.	45
Figure 20 Comparison between the gas bubbles inside a PAC4 solution (left) and in water (right) at a gas fraction of 0.0984.	45
Figure 21- Flow pattern between the two pressure taps at 0.2; 0.5; 1.0; 1.5; 2.0; 2.5; 3.0 SPLM of gas (air) for the swagelok nipple 1/16 inch injector [8]	47
Figure 22 Flow pattern between the two pressure taps at 0.2; 0.5; 1.0; 1.5; 2.0; 2.5; 3.0 SPLM of gas (air) for the gas sparger with sintered filter cartridge injector	47
Figure 23 Comparison of average increase in apparent weight of the pendulum as a function of gas fraction for two different gas injectors	48
Figure 24 Pendulum becomes weightless as injection rate increases	49
Figure 25 Steel bar	50
Figure 26 Bobbles attaching on the bob.	51
Figure 27 Average experimental apparent weight of the pendulum measured by the force sensor as a function of injection rate	53
Figure 28 Differential pressure as a function of gas injection rate	54
Figure 29 Gas fraction measured by the Liquid Level Method, with and without correcting for gas expansion	55
Figure 30 Comparison between the liquid level method and the differential pressure method	56
Figure 31 extrapolation of the gas fraction found by the liquid level method	57
Figure 32 Gas fraction in the pipe as a function of gas injection rate	58
Figure 33 Expected apparent weight vs average experimental force at different gas fractions.	59

Figure 34 Average experimental apparent weight vs average experimental differential pressures for different gas injections.....	61
Figure 35 forces affecting the apparent weight of the pendulum (experiment 1)	64
Figure 36 Different forces that affects the apparent weight of the pendulum.....	65
Figure 37 FFT analysis for left) 0.2 SLPM right) 7.4 SLPM.....	67
Figure 38 a PASCO 850 universal interface, 6-pin mini-DIN connector and PASCO 5N Load Cell PS-2201	72
Figure 39 Mark-10 M5i indicator and a R03-05 force sensor.....	73
Figure 40 Alicat Flow meter calibration data sheet	74
Figure 41 The Feasibility setup with the PASCO 5N Load Cell PS-2201	81
Figure 42 Sowing thread sticking to the pipe.....	82
Figure 47 The steel bar inside the flow loop	82
Figure 48 Mark-10 front panel	83
Figure 49 Labview block diagram	84
Figure 50 Reduction in error from calibration of the differential pressure gauge	85
Figure 43 forces affecting the apparent weight of the pendulum (experiment 2).....	86
Figure 44 forces affecting the apparent weight of the pendulum (experiment 3).....	86

1. Introduction

1.1 Background and objective

Measuring the in-situ gas fraction in a flow is of importance during gas lift operations. A wide variety of gas fraction measuring methods have been developed, based on different principles. But there is still a need for new methods to measure the fractions in exact, fast and simple ways. The method for measuring gas fraction presented in this thesis is a new and innovative method with a simple setup. The idea is to measure the gas fraction through measuring buoyance in a flowing fluid by the use of an object attached to a buoyancy sensor. No existing studies was found in the literature about measuring gas fraction this way. The basic equipment needed for the method presented in this thesis is a pipe filled with liquid, gas and an object attached to a force sensor.

1.2 Experiments and project work

To test if it is possible to measure gas fraction in gas-liquid flows by using a buoyancy sensor, a small-scale simple feasibility setup was designed. Experiments in the feasibility setup showed promising results, which led to further testing and research in a more extensive experimental setup. Before converting the feasibility setup to a more extensive experimental setup, different equipment was tested to find an adequate experimental setup. The method for measuring the gas fraction inside the pipe by using a buoyancy sensor was further developed.

The method used is based on using a force sensor to measure the apparent weight of an ideally stationary object. The object is attached to the force sensor like a pendulum, and immersed in a fluid filled pipe. The gas fraction inside the tube is controlled by injecting gas from the bottom of the pipe. Theory related to buoyancy is used to find the gas fraction inside the pipe by the apparent weight of this pendulum measured by the force sensor. To verify the gas-fraction in the pipe, the in-situ gas fraction calculated from readings of the liquid level of fluid inside the pipe and by using a differential pressure gauge simultaneously in the experimental setup are compared.

1.3 Structure and content

This thesis has theory as the point of departure and shows how theory can be applied to test out a new method through experiments in a laboratory. The thesis is organized as follows:

Chapter 2: Theory

In this chapter the basic theory used to develop the new method, an applicable experimental setup and methods for analyzing the experimental data is introduced. The theory that will be introduced is buoyancy, the dynamic system of a pendulum, two-phase flow in vertical pipes concerning flow regimes and pressure gradients.

Chapter 3: Experimental Part

This chapter contains a short description of the feasibility setup that was designed, and how the feasibility experiments were executed. Furthermore, it contains a more detailed description of the more extensive experimental setup, software used in the experiments with necessary modifications of the software. Followed by an implementation the final experiments.

Chapter 4: Analytical methods

In this chapter the theory from Chapter 2 is used to derive methods for analyzing and comparing the experimental data from the force sensor, the differential pressure gauge used during the experiments and the liquid level measurements of the fluid inside the pipe.

Chapter 5: Results and discussion

The experiments that were done in the feasibility part of the study is considered fully integrated in my research, and gave some interesting answers. Consequently, the results from the feasibility experiments and the results from the main experiments are analyzed and discussed together. The results and discussion part of the thesis is divided into two parts. The first part describes and discusses the changes that were made to the experimental setup as a result of analyzes of the feasibility setup experiments. This part also includes changes necessary due to problems that occurred when converting from the simple small scale feasibility experiments to the more extensive experimental setup.

The second part is an analysis of the adequacy of the experimental setup in relation to the objective of the study. In this part the experimental data from the differential pressure gauge and the liquid level measurements of the fluid in the pipe is compared with data gathered with the new proposed method.

Chapter 6: Error! Reference source not found.

This chapter contains a conclusion from the experimental work and the discussions done in this thesis. Based on the results of the experiments, the potentials of the proposed new method are

concluded on. This includes a summary of issues of uncertainty and shortcomings of the experimental setup, which is considered as important input to further research and development.

Chapter 7:Future studies

In Chapter 7 suggestions for further research and future studies are presented. To succeed, the new method needs to be further tested under a wider variety of experimental conditions and input variables.

Finally, important figures and tables that give a deeper understanding and more in-depth information about the analyses and discussions done in the thesis are given in appendixes. This also includes specifications of the equipment that has been used during the experiments. The appendix also contains Nomenclature defines and explains the abbreviations that are used.

2. Theory

In this chapter the basic theory used to develop methods for analyzing the experimental data is introduced. In order to calculate gas fractions and analyze the experimental data from the apparent weight of the pendulum measured by the force sensor, basic knowledge of buoyancy theory is required, and will therefore be presented in this chapter. Theory of the dynamics of a pendulum will be introduced to give an understanding of why it is important to have a pendulum in rest when measuring buoyancy. During the experiments gas is injected from the bottom of a water filled pipe. As mentioned in the Introduction, two methods are used to verify the gas fraction in the flowing system. These two are calculations of gas fractions by reading of the liquid level of the fluid in the tube, and using a differential pressure. This means that some understanding of multiphase flow and pressure gradients is required. I will start this presentation of relevant theory with Buoyancy theory.

2.1 Buoyancy (Archimedes principle)

If a bubble of air is released inside a pipe of water, the air bubble will always go towards the surface. This is due to a buoyant force that works on the gas bubble and pushes it upwards. Buoyancy is caused by differences in pressure that are acting on opposite sides of an object, and is described by The Archimedes' principle as "The magnitude of the buoyant force on an object always equals the weight of the fluid displaced by the object". [1]

For a better understanding of what buoyancy is, we must look at and understand the physics behind the phenomena buoyancy. The physics behind the buoyant force can be understood by looking at the pressure. When looking at the pressure in a stagnant fluid, the pressure at the bottom is always greater than the pressure at the surface. This can be explained by determining the pressure at a point as[1]:

$$P = P_0 + \rho_{fluid}gh \quad \text{Equation 2.1}$$

Where P_0 is the atmospheric pressure or a reference pressure, ρ is the density of the fluid, g is the gravity and h is the distance from a reference point going downwards. From this equation,

we see that a higher density gives a higher pressure. Also, that the deeper we go, the higher the pressure. Therefore, if an object is placed in a fluid the pressure at the bottom of the object, P_{bot} , will be greater than the pressure at the top of the object, P_{top} . More about pressure and how the pressure can change in a fluid, will be explained by pressure gradients in Chapter 2.4. If considering an object shaped as the cube illustrated in Figure 1, there will be a downwards force acting on the top of the cube equal to the pressure on top of the cube multiplied with the areal (A) of the cube. On the bottom of the cube, a force will be acting upwards equal to the pressure at the bottom multiplied with the areal. The difference between these forces is the buoyant force (F_B), and is given in Equation 2.2 [1].

$$F_B = (P_{bot} - P_{top})A \quad \text{Equation 2.2}$$

By inserting Equation 2.1 into Equation 2.2 we get:

$$F_B = (\rho_{fluid}g(h_{bot} - h_{top}))A \quad \text{Equation 2.3}$$

The volume of the cube will be the displaced volume of the cube given as:

$$V_{disp} = (h_{bot} - h_{top})A \quad \text{Equation 2.4}$$

By inserting Equation 2.4 into Equation 2.3, we will get a formula for buoyancy (Equation 2.5)[1] that is dependent on the volume fluid displaced (V_{disp}) by the cube.

$$F_B = \rho_{fluid}gV_{disp} \quad \text{Equation 2.5}$$

Since the density multiplied with the volume fluid displaced by the object, is equal to the mass of the fluid displaced (m), the buoyancy becomes equal to the weight of the fluid displaced (mg).

$$m = \rho_{fluid}V_{disp} \quad \text{Equation 2.6}$$

$$F_B = mg \quad \text{Equation 2.7}$$

This correspond to the Archimedes principle.

Since the pressure on the bottom will always be higher than on the top, the buoyant force will always act upwards on an object. Another force acting on the object is the gravity force (F_g). The forces acting on a submerged object is illustrated in Figure 1.

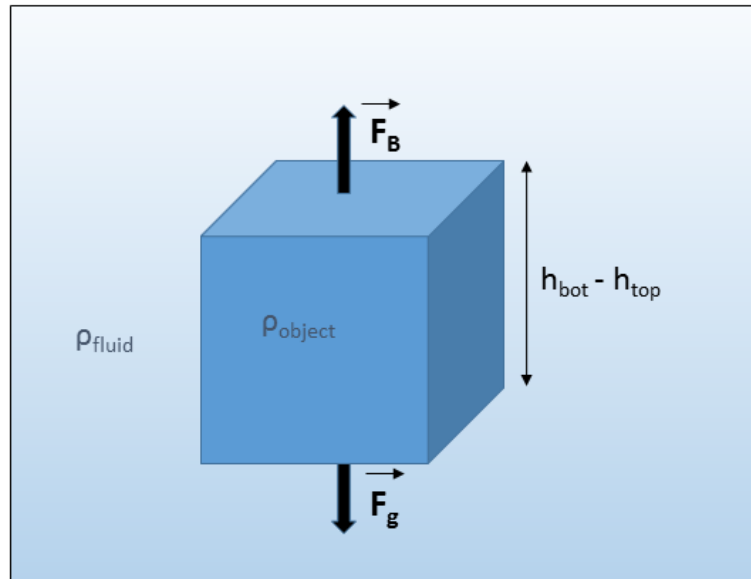


Figure 1 Forces acting on a submerged object

Whether an object will sink or go towards the surface depends on the density of the object compared with the density of the fluid. If the objects density is larger than the density of the fluid, the object will sink. This means that the gravity force applied to the object is greater than the buoyant force. If the density of the object is smaller, the object will be pushed upwards to the surface. In the latter case, the buoyant force applied to the object is larger than the gravity force acting on the object. If the buoyant force is equal to the gravity force the object is in equilibrium, and will not move up or down. The gravity force of an object is the true weight of the object. An object submerged in a static fluid have an apparent weight (W') which is equal to the true weight (F_g) of the object minus the force reduced by the buoyancy. [1]

$$W' = F_g - F_B \quad \text{Equation 2.8}$$

The difference between the true weight and the apparent weight of an object is illustrated in *Figure 2*. In *Figure 2a* a cube is connected to a force sensor where the cube is surrounded by air. In this case, the force sensor measures the gravity force of the object, which is the true weight of the object. In *Figure 2b* the object is submerged in a fluid. The force sensor now measures the apparent weight of the object.

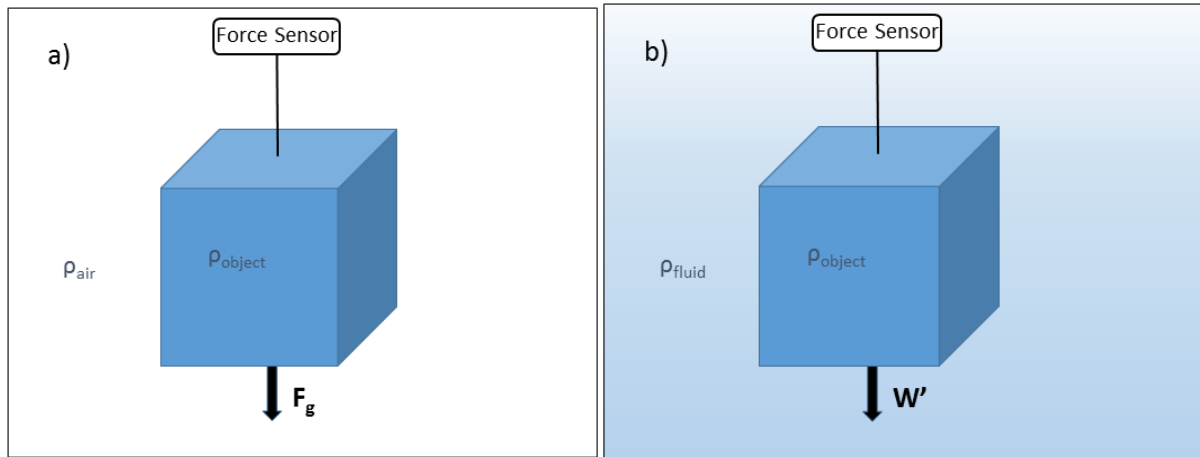


Figure 2 Difference between a) the true weight of an object and b) the apparent weight of an object

The relations described above can be used to measure the volume of an object and the density of the fluid surrounding a submerged object. This can be done by measuring the force of the object suspended in air, and comparing it with the apparent weight of the object suspended in a fluid. I will now shortly proceed with theory of dynamics of a pendulum of relevance for my experiments.

2.2 Dynamic systems of a pendulum

A pendulum consists of a bob attached to a string that is hanging from a pivot. A figure of a pendulum is shown in *Figure 3*. Here we have a bob with the mass m , suspended with the force F_T by a light string with the length L . The figure illustrates that the body is swinging. When a pendulum is at rest (stationary) the force acting on the string (F_T) from the bob is dependent on the gravity force, $F_T = F_g = mg$, where g , is gravity. When the pendulum is swinging, the mass center is moving and the force acting on the string becomes dependent on a tangential force $F_T = mg \cos \theta$. θ is the angle in radians between the string when the system is at rest and when the pendulum is swinging. This means that as the pendulum moves, the force acting on the string will oscillate.

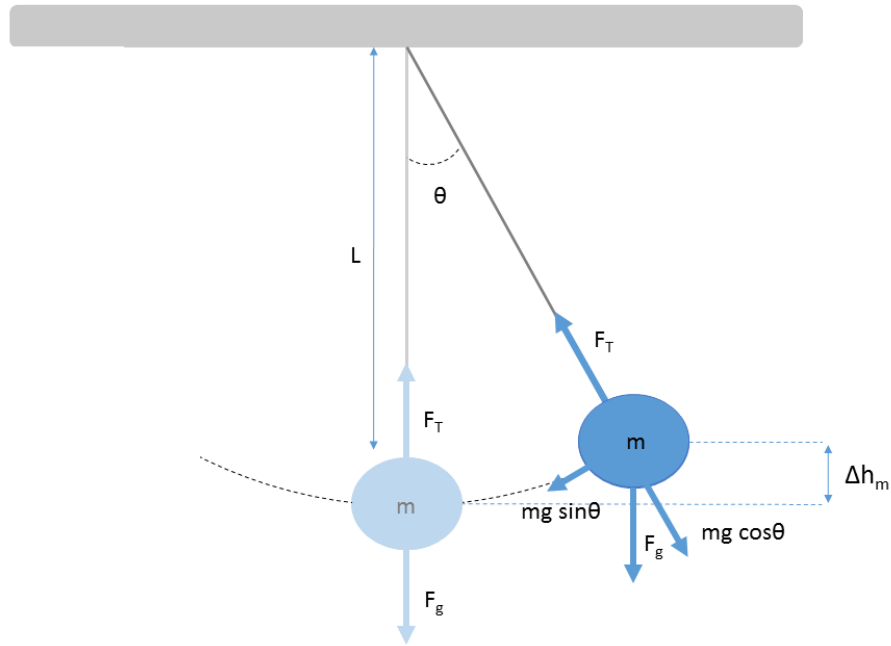


Figure 3 Forces acting on a pendulum

The experiments in this thesis are conducted in a vertical pipe filled with water and injected with gas at different injection rates. Therefore, two-phased flow in a vertical pipe will be discussed in this theory chapter. Only dispersed bubble flow and slug flow will be tested in the experiments, therefore, the dispersed bubble flow and slug flow will be shortly introduced.

2.3 Two phase flow regimes in upward gas-liquid flow in vertical pipes

Flow regimes in vertical pipes behave a little different than in horizontal pipes, due to the direction of gravity. The different flow regimes that can occur in a vertical pipe are slug flow, churn flow, dispersed bubble flow and annular flow [2]. These flow regimes are illustrated in *Figure 4*.

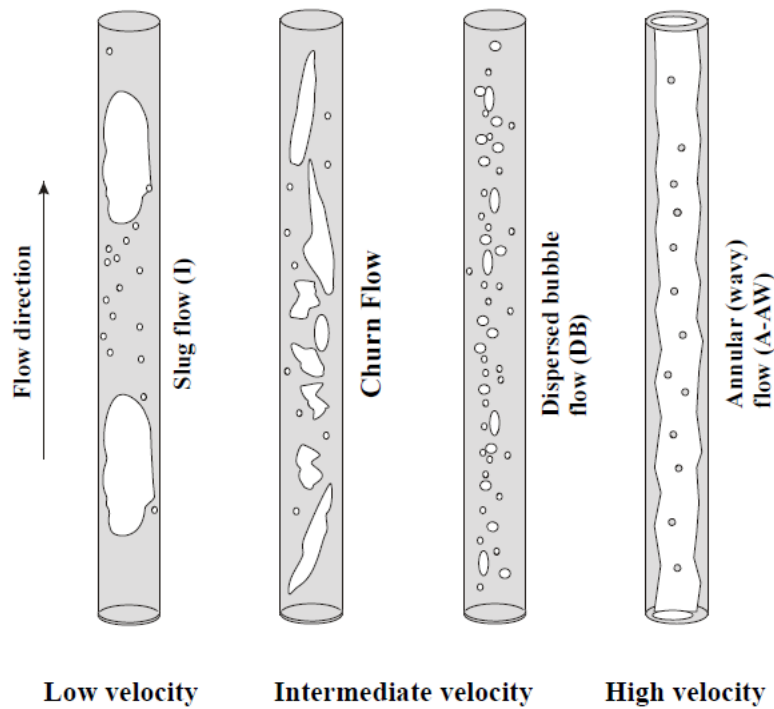


Figure 4 Flow regimes in vertical pipes for two-phase flow.[2]

The flow regime that is present in a pipe depend on flow rates, fluid properties and the size of the pipe. [3]. Figure 5 shows a flow regime map, which illustrates the different flow regimes that may occur with different superficial gas and liquid velocities in vertical pipes.

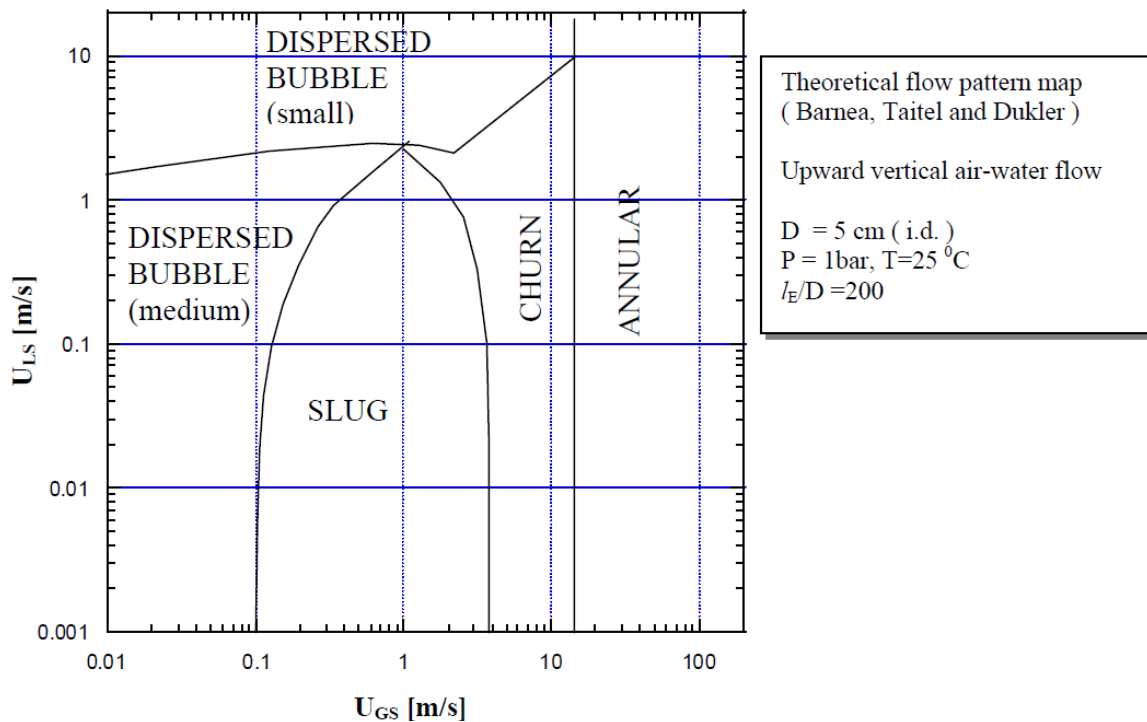


Figure 5 Flow regime map in vertical pipes for two-phase flow.[2]

Dispersed bubble flow(medium) occurs when the superficial gas velocity is low, which can be seen in the flow regime map in Figure 5. If the superficial gas velocity increase the bubble flow will eventually break down as the bubbles merge into Taylor bubbles. When Taylor bubbles occurs the flow regime is called slug flow.

2.4 Pressure gradients

The pressure gradient $\left(\frac{dp}{dx}\right)$ for flow in a pipe depends on the pipe diameter (D), the fluid viscosity (μ), the fluid density (ρ), the flow velocity (U), the roughness of the pipe (ϵ) and the inclination of the pipe (β). The pressure gradient is a summation of three different terms. The frictional pressure gradient $\left(\frac{dp}{dx}\right)_f$, the hydrostatic pressure gradient $\left(\frac{dp}{dx}\right)_h$ and the acceleration pressure gradient $\left(\frac{dp}{dx}\right)_a$. Which gives Equation 2.9[2].

$$\left(\frac{dp}{dx}\right) = \left(\frac{dp}{dx}\right)_f + \left(\frac{dp}{dx}\right)_h + \left(\frac{dp}{dx}\right)_a \quad \text{Equation 2.9}$$

This section presents the three different pressure gradient terms for a two-phase fluid mixture (m) when using the homogeneous two-phase pressure drop model [2]. This means that homogenous fluid properties are assumed for the two phases.

In two-phase flow the frictional pressure drop, the hydrostatic pressure gradient and the hydrostatic pressure gradient are given in Equation 2.10, Equation 2.11 and Equation 2.12, respectively.

$$\left(\frac{dp}{dx}\right)_f = \frac{4}{D} \cdot C(\text{Re}_m)^{-n} \cdot \frac{1}{2} \rho_m U_{\text{mix}}^2 \quad \text{Equation 2.10}$$

$$\left(\frac{dp}{dx}\right)_h = \rho_m g \cos\beta \quad \text{Equation 2.11}$$

$$\left(\frac{dp}{dx}\right)_a = -\rho_m U_{\text{mix}} \cdot \frac{dU_{\text{mix}}}{dx} \quad \text{Equation 2.12}$$

In the equations, the constant $C= 0.046$ and $n=0.2$. β is relative to the vertical direction and the Reynolds number to the mixture (Re_m) are given as[2]:

$$\text{Re}_m = \frac{\rho_m U_{\text{mix}} D}{\mu_m} \quad \text{Equation 2.13}$$

After having presented the basic theories that are the basis for the chosen methodology, an overview of the experimental setup will follow.

3. Experimental Part

In this chapter, the equipment and the procedures necessary to perform the experiments are presented. To perform the experiments, a pendulum attached to a force sensor was immersed into a pipe filled with water. Gas was injected from the bottom of the pipe to change and control the amount of gas inside the pipe. The purpose of the experiments is to measure the apparent weight of the pendulum as the gas inside the pipe changes. This chapter contains a short description of the feasibility setup, and how the feasibility experiments were executed. Then follows a description of the more extensive experimental setup, the software used in the experiments with necessary modifications of the software. Followed by an implementation the final experiments.

3.1 Feasibility test

Before running the experiments on a large scale, a simple smaller scale feasibility test setup was built to see if using buoyancy to measure gas fraction in a pipe is possible, to test the equipment and to see if any adjustments to the setup, pendulum and/or fluid used were necessary. As mentioned in the introduction the feasibility experiments are considered fully integrated in my research, and the results will be analyzed and discussed together with the results from the main experiment.

3.1.1 Setup feasibility test

The equipment used to build the feasibility test set up is presented below, and the setup is shown as a sketch in *Figure 6*.

Equipment needed:

1. Pendulum, which consist of a string and a bob
2. Water
3. Gas supply

4. A rigid system to mount the force sensor
5. Force sensor
6. Vertical pipe, with a closed bottom and with the possibility for connecting gas supply on the bottom
7. Gas sparger with a sintered filter cartridge

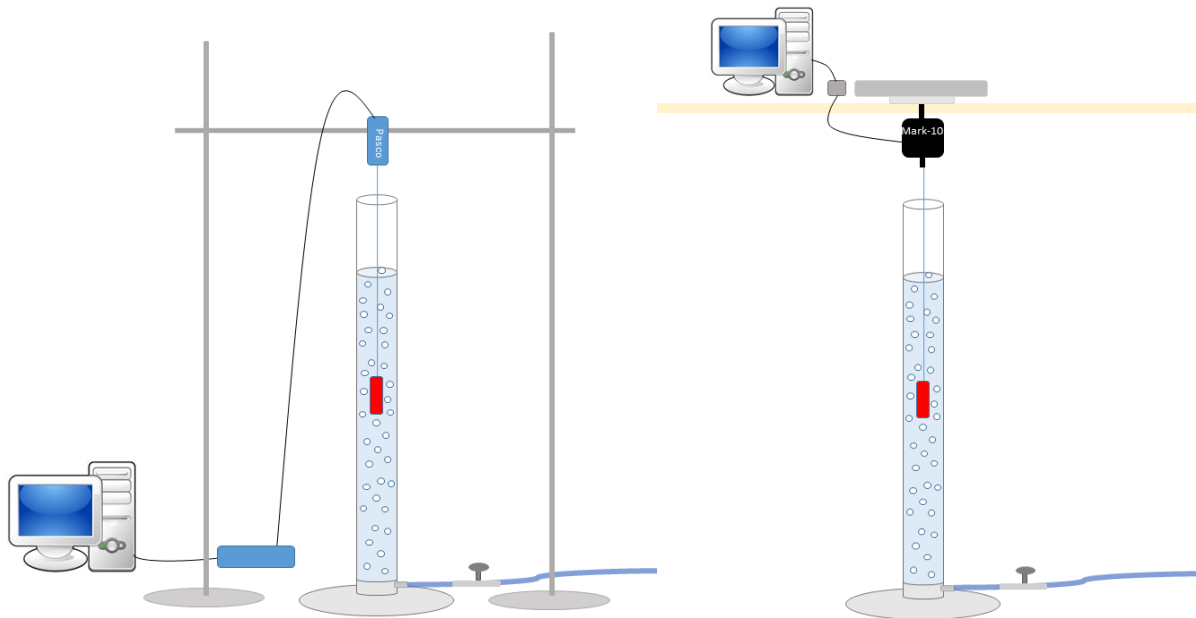


Figure 6 Feasibility test set up for a) PASCO force sensor and b) Mark-10 force sensor

A transparent acrylic pipe, which was placed vertically onto a plate made by PVC, was used to build the feasibility setup. The vertical pipe has a height of 60 cm, an inner diameter of 4.0 cm and a wall a thickness of 0.5 cm. Near the bottom of the vertical pipe, a gas sparger with a sintered filter cartridge, was attached inside the pipe and connected to a gas supply. The gas supply used is a hose with a needle valve, which is connected to an underground gas compressor system at UiS. To be able to account for the volume of fluid inside the pipe a printable ruler on a transparency film was pasted on the side of the pipe.

A force sensor was placed straight above the vertical pipe. Two different force sensors were used in the feasibility test. One sensor from PASCO and one force sensor from Mark-10. More specifications about the force sensors can be found in Appendix A. The pendulum was attached to the force sensor and placed inside the pipe. Figure 6a illustrates the set up when using a force sensor from PASCO and Figure 6b illustrates the setup when using a force sensor from Mark-10. Since the force sensors has different assemble equipment, mounting the equipment needed two different set ups. The force sensors form PASCO was mounted between two tripods. The force sensor from Mark-10 was mounted to an acrylic glass plate, with screws provided from

Mark-10. The acrylic glass plate was placed on a table with a heavy lead block on top to prevent movement of the force sensor. The force sensor was then connected to a computer with adequate equipment. Information about this equipment and pictures of the force sensors can be found in Appendix. The program PASCO Capstone was used to log the data from the PASCO force sensors. MESURgauge logs the data from the Mark 10-force sensor.

3.1.2 Feasibility test method

After setting up the feasibility test as described in the previous chapter, the pipe is filled with water up to a certain volume V_w , which corresponds to a height, h_w , on the pipe (illustrated in Figure 7). The water must be filled above the bob and the water height noted. Before the experiment can start, the measuring frequency and the tare weight need to be set. In the feasibility test, the tare weight was set as the weight of the pendulum immersed in water. The measuring frequency was set to maximum (50 Hz in PASCO Capstone and 50 readings per second in MESURgauge).

The PASCO Capstone/MESURgauge program is then started, and the data acquisition from the force sensor thereby initiated. After about a minute, the time interval when running the experiment without gas injection is noted. The gas injection is then turned on to a low gas injection rate by barely opening the needle valve. The gas injection rate will correspond to a certain mixed fluid (water and gas) height, h_{m1} on the pipe. The time interval for when the injection rate is set equal to a fluid height of h_{m1} is noted, before increasing the injection rate to a mixed water and gas fluid height h_{m2} . This procedure was followed until the final injection rate was reached, which corresponds to the fluid height h_{mn} . The gas fraction can then be calculated by the change in mixed fluid height by using the “liquid level” method described in Chapter 4.4.2. By knowing the time interval for each gas injection, the force registered by the software used can now be compared with the calculated gas fraction. A MATLAB code used for calculation and comparison can be found in Appendix B

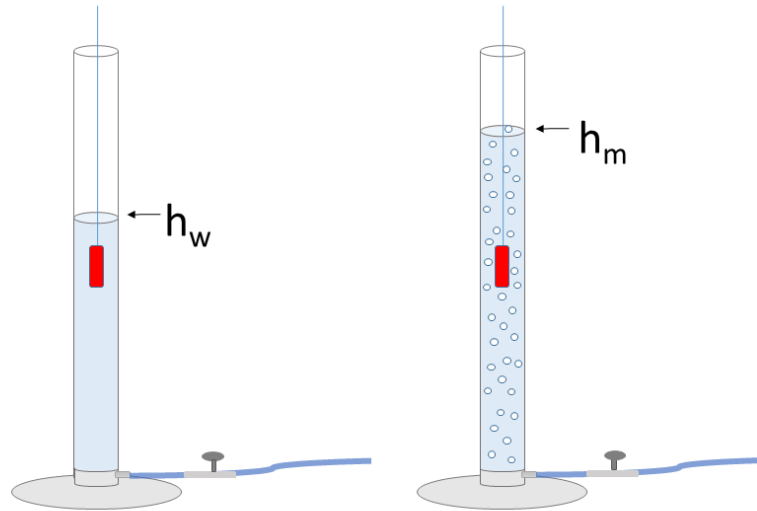


Figure 7 Feasibility set up with a) no gas injection B) gas injection

Before discussing the experiences with the feasibility setup, the modifications that were done and the main experimental setup, the next sections will give an overview of the main experimental setup.

3.2 Main experimental setup

The main experimental setting is illustrated in Figure 8. The blue lines in the figure illustrate pipes filled with water, the red lines illustrate pipes filled with gas and the black lines illustrate electrical cables connecting the different transmitters to the computer. The experimental set up, as shown in Figure 8 consists of the components listed below, and will be further described and commented on in the sections and chapters below:

- Flow loop
- Gas flow meter
- Gas pipes
- Force sensors
- Pendulum
- Valves
- Pressure sensors
- Computer and software programs

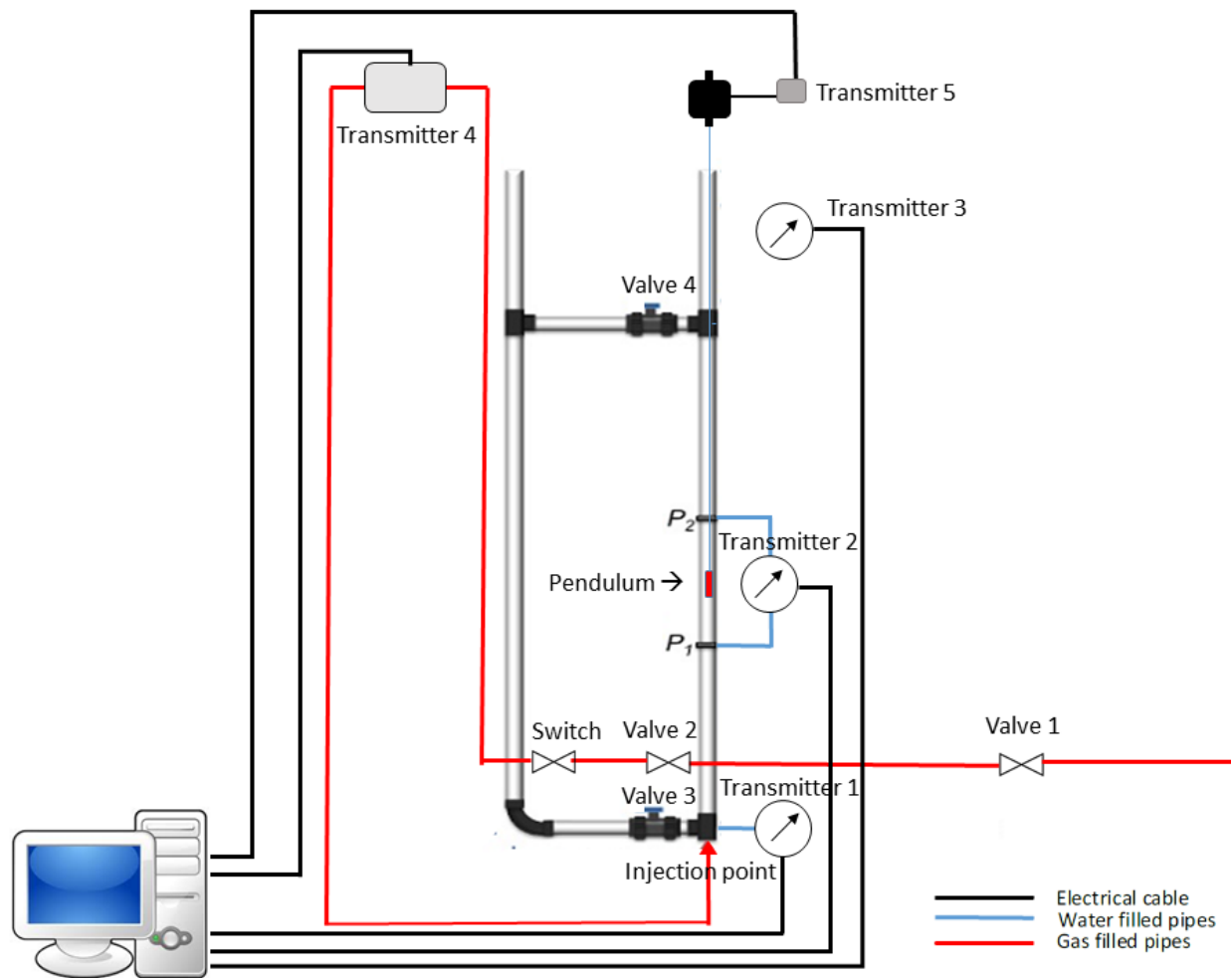


Figure 8 Flowchart of the setup with data logging

In Figure 8 the blue lines illustrates pipes filled with water, the red lines illustrate pipes filled with gas and the black lines illustrate electrical cables connecting the different transmitters to the computer. The experimental set up, as shown in Figure 8 consists of the components listed below, and will be described in this chapter:

- Flow loop
- Gas flow meter
- Gas pipes
- Force sensors
- Pendulum
- Valves
- Pressure sensors
- Computer and software programs

3.2.1 Flow loop with pressure gauges

Figure 9 shows a sketch of the flow loop that was used to perform the experiments.

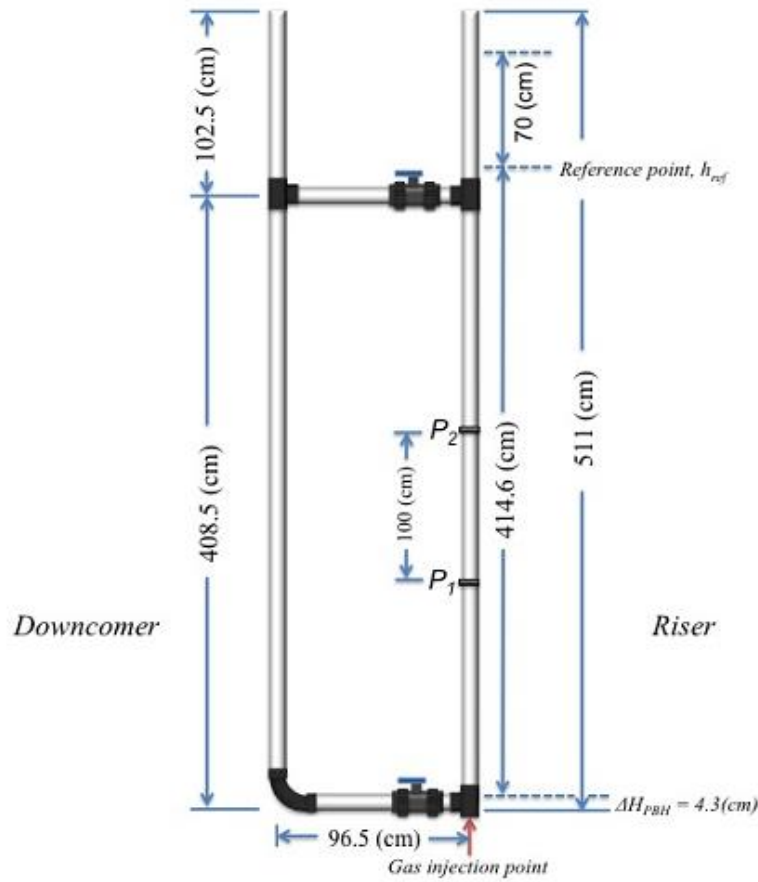


Figure 9 Illustration of the flow loop[4]

The flow loop consists of two 511 cm long vertical transparent acrylic pipes and two 96.5 cm long horizontal transparent acrylic pipes. The pipes have an inner diameter of 4.0 cm and an outer diameter of 5.0 cm. The vertical pipe on the right-hand side is called the riser and the vertical pipe on the left-hand side is called the downcomer. The riser and the downcomer are connected by the two horizontal pipes illustrated in Figure 9.

On the bottom of the riser there is a gas injection point. The gas injection point is connected to a flow meter, which gives the opportunity to inject gas with different injection rates into the riser. Due to the position of the injection point, the flow in the pipe will go upwards in the riser and downwards in the downcomer, which is the reason for their names. Two valves (valve 3 and 4 in Figure 8) are placed on the horizontal pipes close to the riser. These valves give the opportunity to close the flow loop, and only use the riser as a horizontal pipe. A measuring tape is attached to the top of the riser to account for fluid height in the pipe.

On the riser, there are 4 pressure taps connected to transmitter 1, 2 and 3. Transmitter 1 is a Crystal Digital Test Gauge XP manometer connected to a pressure tap that is measuring the

bottom hole pressure in the pipe. Transmitter 2 is a Rosemount transmitter 3051C, and is connected to two of the pressure taps, marked P_1 and P_2 in Figure 9. Transmitter 2 measures the differential pressure between the two pressure taps. The pressure taps are placed 100 cm above the gas injector. The distance between P_1 and P_2 are 100 cm, which is illustrated in the figure. Transmitter 3 is connected to a Rosemount transmitter and measures the atmospheric pressure

3.2.2 Flow meter, gas pipes and pressure gauges

The red lines in Figure 8 represent the gas lines. The gas is transferred from an underground gas compressor system at UiS, and is turned on by valve 1. The gas is transferred from valve 1 to valve 2, which is a gas inlet regulator. The gas inlet regulator will be fully open during the experiments. Further, the gas goes to the switch, which is a three-way valve, that can be set to open, closed or bleeding out. When the three-way valve is open, the air is transferred to transmitter 4, which is a flow meter. The flowmeter used for these experiments is a MCR-50SLPM-D flowmeter from Alicat Company. Specifications of the flow meter can be found in the Appendix. The flow meter transfers the gas to the gas injection point, which delivers the gas into the flow loop.

3.2.3 Force sensor and pendulum

A Mark-10 MR03-05 Force Sensor is mounted to a beam straight above the center of the riser. The force sensor is connected to a M5i Indicator, which is marked as transmitter 5 in Figure 8. The pendulum is hoisted down the riser, between the two pressure taps that are measuring the differential pressure and then attached to the force sensor.

3.3 Software

The software used is LabVIEW, MESURgauge, MATLAB and Excel. LabVIEW and MESURgauge are the programs used for data acquisition. In LabVIEW, the differential pressure, the atmospheric pressure, the Alicat outlet pressure, the gas injection rate and the temperature are registered continuously through the experiments. Before using LabVIEW, some modifications to the existing program was necessary to simplify the experimental procedure. The modifications done are described in the following section. MESURgauge

registers the force measured by the force sensor. Excel and MATLAB are programs used for analyzing the data. Excel is used to read the log files created by LabVIEW and MESURgauge. Both Excel and MATLAB are used as calculation programs and to plot graphs. The MATLAB codes used and a front panel of the MESURgauge program can be found in the Appendix.

3.3.1 Modification of the LabVIEW program

As mentioned some modifications of the already existing LabVIEW program at UiS was performed. The program was given the ability to automatically increase/decrease the gas injection rate at a desired time interval. The front panel of the LabVIEW program is shown in Figure 10. The working scheme (block diagram) can be found in the Appendix.

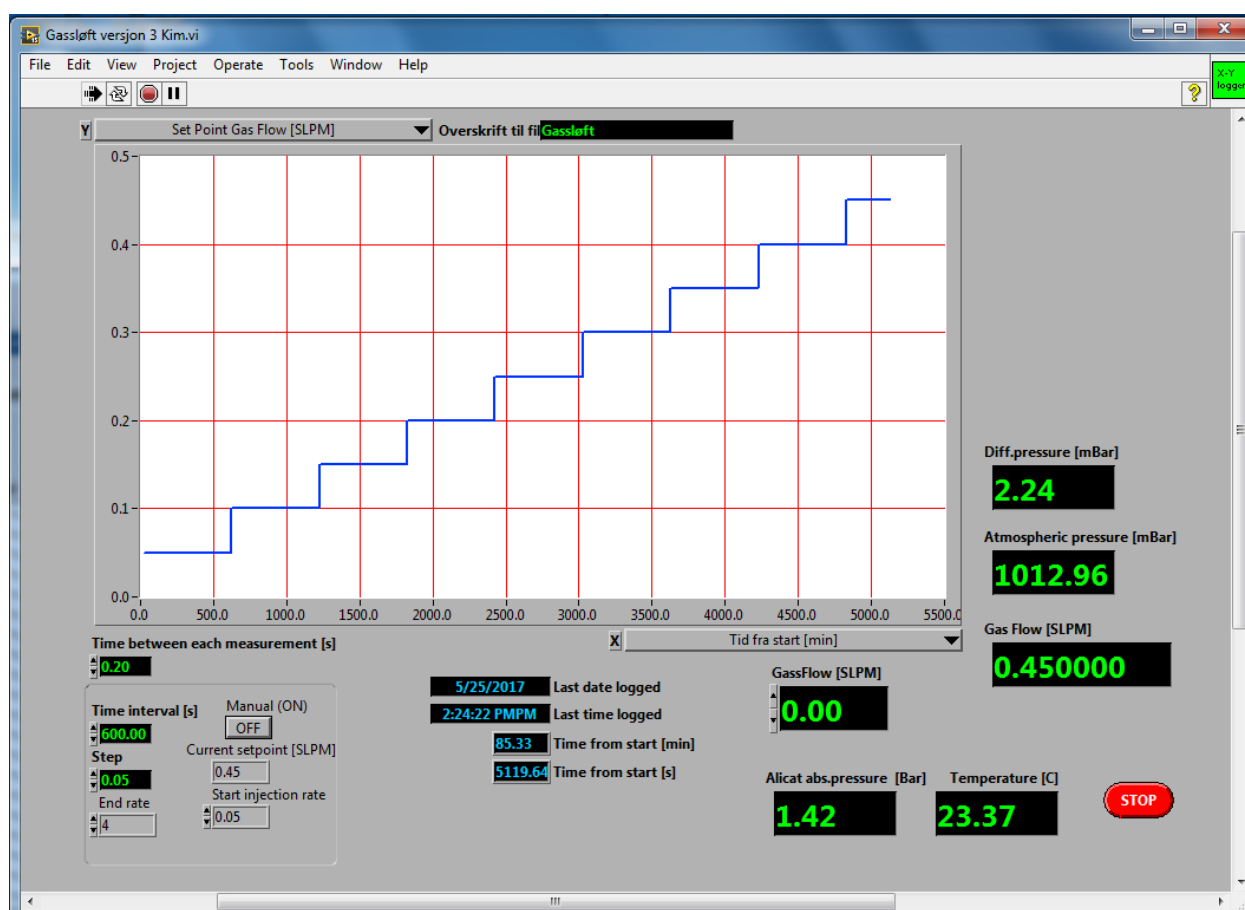


Figure 10 LabVIEW front panel

The modified program now has two options, manual and automatic. There is an on/off switch in the program. “ON” means that the program is run manually. Then the gas flow rate can be chosen by changing the value in the “GassFlow [SLPM]” box. If the “ON/OFF” switch is “OFF”, the program is set to automatic. Before running the program, the following input values, which can be found in the left lower corner in the LabVIEW program, must be set:

- **“Time interval [s]”**: Sets how many seconds the program shall run before changing the gas injection rate.
- **“Step”**: Gives the increase/decrease of the gas injection rate for each time interval in SLPM
- **“Start injection rate”**: Lets the program know which gas injection rate in SLPM to start injecting.
- **“End rate”**: Tells the program at which gas injection rate to stop increasing the gas injection rate.

The current gas injection rate can be seen in “Current set point [SLPM]”.

The other “boxes” in the program are the series of parameters that are being logged:

- **“Diff. pressure”**: Differential pressure in mBar
- **“Atmospheric pressure [mBar]”**: Atmospheric pressure in mBar
- **“Gassflow [SLPM]”**: Injection rate in SLPM
- **“Alicat abs.pressure[bar]”**: Alicat outlet pressure in bar
- **“Temperature[C]”**: Ambient temperature in °C
- **“Time between each measurement [s]”**: Time interval between each measurement in seconds
- **“Time from start [s]”**: Time from start in seconds

The logged values are saved in a file that can be opened in Excel.

3.3.2 Changes in the LabVIEW programs due to technical problems

While running the experiments, there was a problem with the connection from the Crystal Digital Test Gauge XP2i manometer (transmitter 1) and the LabVIEW program. This problem caused LabVIEW to stop and the computer had to be restarted to continue to use LabVIEW.

The reason for this error is currently unknown. Since the bottom hole pressure is almost

constant through the experiments, the connection between the pressure gauge and LabVIEW was removed. The bottom hole pressure was manually noted before each experiment.

3.3.3 Calibration the differential pressure gauge

To reduce the error for the differential pressure gauge, a calibration of the Rosemount transmitter 3051C was done. The pressure gauge is marked with a maximum differential pressure range of 62.27 bar, which was set to -31.13 mbar to 31.13 mbar. Since there are only positive differential pressure values in the experiments in this thesis, the pressure range was reduced to -1mbar to 36.2 mbar. The result from this calibration can be found in the appendix.

3.4 Running the experiments

Before starting the experiments, the valves on the flow loop must be closed. The riser is then filled with water up to a certain height h_w in the riser. This should preferably be done the day before to ensure room temperature. All pipes from the pressure taps to the pressure gauges must be filled with water, and checked for air bubbles. These pipes are indicated in Figure 8 as “pipes filled with water”. All the valves connected to the gas filled pipes described in Chapter 3.2.2 is opened. The Mark-10 M5i indicator is turned on. The indicator is set to measure in Newton and tared, before attaching the pendulum. The setup is now ready to run.

The input values on LabVIEW described in chapter 3.3.1 is set, typically as shown in *Figure 10*. The measuring frequency in MESURgauge is set to 50 readings per second. The LabVIEW and MESURgauge programs are then started simultaneously.

The input values in LabVIEW used for the three final experiments are given in *Table 1*. The input values in experiment 1 were changed during the experiment to reduce the time duration of the experiment.

Experiment Nr	<i>Time interval [s]</i>	<i>Step [SLPM]</i>	<i>Start injection rate [SLPM]</i>	<i>End rate [SLPM]</i>	<i>Duration</i>
Experiment 1.1	600	0.1	0.1	4.2	9h, 50min
Experiment 1.2	600	0.2	4.4	7	
Experiment 1.3	600	-	7.5	7.5	
Experiment 2	600	0.2	0.2	5.8	4h, 50min
Experiment 3	600	0.2	0.2	7.4	6h, 10min

Table 1 LabVIEW input values for the three final experiments

4. Analytical methods

In order to analyze the data from the experiments the theory from Chapter 2 is used to derive methods for analyzing and comparing the experimental data from the force sensor, the differential pressure gauge used during the experiments and the liquid level measurements of the fluid inside the pipe. This chapter will also give explanations on how the differential pressure gauge work. The formulas and methods explained will be used in the result and discussion part (chapter 5)

4.1 Finding the volume of the bob

In order to find the expected buoyancy acting on the pendulum during the experiments, the volume of the bob must be known. The volume of the bob was found by using buoyancy. The contribution of weight and volume of the string has been considered insignificant and neglected in these calculations.

By measuring the true weight of the pendulum and the apparent weight of the pendulum submerged in water the volume of the bob can be found by using the buoyancy Equation 2.5 and the equation for apparent weight Equation 2.8. By inserting Equation 2.8 into Equation 2.5, a relation between the volume displaced (V_{disp}), the true weight (F_g) and apparent weight (W') are found:

$$\rho_w g V_{disp} = F_g - W' \quad \text{Equation 4.1}$$

The volume displaced is equal to the volume of the bob (V_{bob}). By solving Equation 4.1 for volume displaced, the volume of the bob can be found by:

$$V_{bob} = V_{disp} = \frac{F_g - W'}{\rho_w g} \quad \text{Equation 4.2}$$

4.2 Experimental data processing

The experimental data must be processed to obtain representative information from the experiments. For processing of the data an average and a standard deviation of the values given for a specific gas injection rate were calculated.

Average value of the data for each injection rate is calculated by:

$$\bar{X} = \frac{1}{n} \sum_{i=1}^n X_i \quad \text{Equation 4.3}$$

Where X_i is an i -th measurement of force (F), gas fraction (ε_g) or differential pressure (p_{diff}) within a specific injection rate, with n number of readings. The Standard deviation is calculated by:

$$SD_X = \sqrt{\frac{1}{n} \sum_{i=1}^n (X_i - \bar{X})^2} \quad \text{Equation 4.4}$$

The results obtained by the calculations are presented in plots in the Result and Discussion chapter

4.3 Differential pressure

To use the differential pressure data, it is necessary to understand how the differential pressure gauge works. In chapter 2.4 the pressure gradients was introduced, in this subsection the pressure gradients will be used together with *Figure 11* to explain how the differential pressure is measured and how to analyze the values logged by LabVIEW.

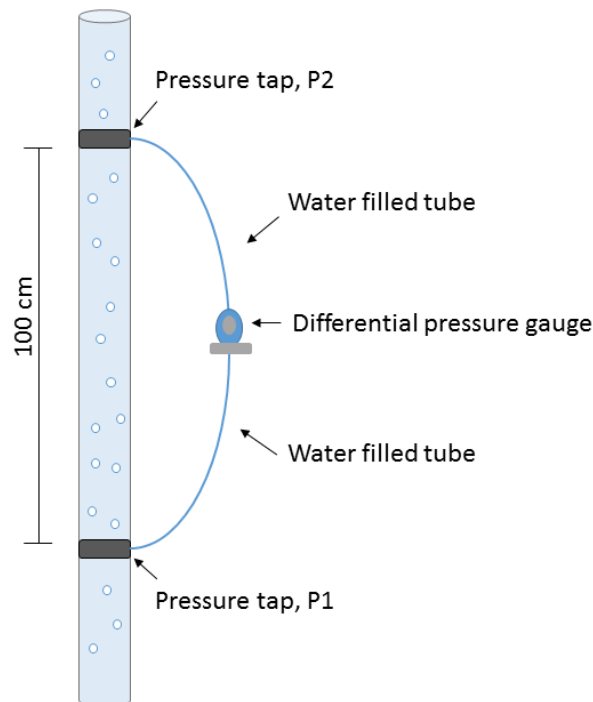


Figure 11 Differential pressure gauge

Figure 11 illustrates how the pressure taps is attached to the raiser and connected to the differential pressure gauge. The differential pressure is measured by the difference between the pressure drop inside the stagnant water filled pipes (ΔP_{pipes}) and the pressure drop between the pressure taps inside the raiser (ΔP_{riser}) [5]. Which gives the differential pressure measured by the pressure gauge:

$$p_{diff} = \Delta p_{tubes} - \Delta p_{riser} \quad \text{Equation 4.5}$$

The pressure drop can be found by using the pressure gradients (Equation 2.10, Equation 2.11 and Equation 2.12) described in chapter 2.4.

The frictional pressure gradient (Equation 2.10) and the acceleration pressure gradient (Equation 2.12) depends on velocity, and will therefore be equal to zero, in a stagnant fluid. The pressure gradient in the water filled pipe will therefore only depends on hydrostatic pressure gradient:

$$\left(\frac{dp}{dx}\right) = \left(\frac{dp}{dx}\right)_h = \rho g \cos\beta \quad \text{Equation 4.6}$$

By knowing that the distance between the two pressure taps is 1 meter ($\Delta h = \cos\beta \Delta x = 1$) the pressure drop inside the stagnant water filled pipes is found by integrating Equation 4.6 from pressure tap1 to pressure tap2:

$$\Delta p_{tubes} = (\Delta p_h)_{tubes} = \rho_w g \Delta h = \rho_w g \quad \text{Equation 4.7}$$

Where ρ_w is the density of water.

In the riser the liquid is flowing in a vertical pipe. This means that the pressure drop in the riser will be affected by all three differential pressure gradients. Since there is no change in the diameter of the pipe, the pressure gradient from the acceleration term may come from increase in bubble size. The acceleration term in such systems can usually be neglected[5, 6]. The pressure gradient inside the riser is then found by:

$$\left(\frac{dp}{dx}\right) = \left(\frac{dp}{dx}\right)_h + \left(\frac{dp}{dx}\right)_f = \rho g \cos\beta + \frac{4}{D} \cdot C(Re_m)^{-n} \cdot \frac{1}{2} \rho_m U_{mix}^2 \quad \text{Equation 4.8}$$

The frictional pressure gradient is dependent on the velocity of the fluid, which is an unknown factor in this system. The frictional pressure drop from the friction gradient will therefore be written as Δp_f . The pressure drop inside the riser is then found by integrating Equation 4.8 from pressure tap1 to pressure tap2:

$$\Delta p = (\Delta p_h + \Delta p_f)_{riser} = \rho_m g \Delta h + \Delta p_f = \rho_w g + \Delta p_f \quad \text{Equation 4.9}$$

Then the differential pressure is then given by:

$$p_{diff} = \rho_w g - \rho_m g - \Delta p_f \quad \text{Equation 4.10}$$

Where the mixture density, for a water and gas system, is given as:

$$\rho_m = \rho_g \varepsilon_g + \rho_w (1 - \varepsilon_g) \quad \text{Equation 4.11}$$

By inserting Equation 4.11 into Equation 4.10, the differential equation as a function of gas fraction can be found:

$$p_{diff} = \rho_w g \Delta h - (\rho_g \varepsilon_g + \rho_w (1 - \varepsilon_g)) g \Delta h - \Delta p_f \quad \text{Equation 4.12}$$

Which gives:

$$p_{diff} = (\varepsilon_g \rho_w - \rho_g \varepsilon_g) g \Delta h - \Delta p_f \quad \text{Equation 4.13}$$

The distance between pressure tap1 and pressure tap2 is 1 meter. The differential pressure as a function of gas fraction then becomes:

$$p_{diff} = (\varepsilon_g \rho_w - \rho_g \varepsilon_g) g - \Delta p_f \quad \text{Equation 4.14}$$

Where, the hydrostatical pressure drop is represented by $(\varepsilon_g \rho_w - \rho_g \varepsilon_g) g \Delta h$

4.4 Determining the gas fraction in the system

To determine the gas fractions in the experiments two methods were used: 1) Using an average of the differential pressure data obtained by LabVIEW which will be called the differential pressure method in this thesis. 2) Reading the changes in liquid level which will be called the liquid level method in this thesis. The two methods are described below and compared in the result and discussion chapter.

4.4.1 The differential pressure method

To find the gas fraction from the differential pressure data, the differential pressure Equation 4.14 is used. By solving Equation 4.14 for gas fraction (ε_g):

$$\varepsilon_g = \frac{p_{diff} + \Delta p_f}{(\rho_w - \rho_g)g} \quad \text{Equation 4.15}$$

As mentioned the frictional pressure drop in the experiments is unknown in section 4.3 . In the experiments, the fluid inside the pipe consists of a rotating liquid with an upward flowing gas. The rotating fluid will have an overall frictional pressure gradient equal to zero, while the frictional pressure gradient will be positive due to flowing gas. Thus, the overall frictional pressure drop is assumed small. To be able to find the gas fraction from the differential pressure the frictional pressure drop is therefore assumed negligible. Which makes the relation between gas fraction and differential pressure:

$$\varepsilon_g = \frac{p_{diff}}{(\rho_w - \rho_g)g} \quad \text{Equation 4.16}$$

If the frictional pressure drop can be assumed negligible will be discussed in the result and discussion chapter.

4.4.2 The liquid level method

Finding the gas fraction in the fluid from the liquid level is done by measuring the height of the fluid in the pipe when no gas is injected (h_w) and comparing it with the height of the fluid when gas is injected (h_m). The gas fraction found from this method is an average gas fraction (ε_{g_ave}) of the fluid in the pipe, and can be found by:

$$\varepsilon_{g_ave} = \frac{V_g}{V_m} = \frac{V_m - V_w}{V_m} = \frac{h_m - h_w}{h_m} \quad \text{Equation 4.17}$$

Where, V_m is volume of mixed fluid, V_w is volume of water and V_g is volume of gas in the pipe. Before using this method three phenomena must be considered. Slugging, gas expansion and change in rise velocity due to gas expansion.

4.4.2.1 Slugging

As the injection rate increase, the flow regime will go from dispersed bubbles into slugging[2]. When slugging occurs, it is more difficult to measure the liquid height, due to a flocculation in liquid height caused by Taylor bubbles. To account for slugging the highest and lowest fluid height in the pipe was measured and marked the average was plotted with error bars.

4.4.2.2 Gas expansion

Due to a decrease in pressure from the bottom to the top of the pipe, the gas will expand as it moves towards the surface. This gives larger gas fraction on the top of the pipe than on the bottom. This might be a problem in long pipes, such as the riser, where the pressure difference

becomes considerable. The gas fraction measured is then the average gas fraction in the whole pipe, and not in-situ gas fraction.

To account for the gas expansion in the riser, the gas fraction was corrected by using Boyle's law [7] which states that pressure times volume is constant:

$$PV = c \quad \text{Equation 4.18}$$

Where P is pressure, V is volume and c is constant.

Boyle's law was used to estimate the relation between the average gas fraction between the in-situ gas fraction with the average gas fraction in the whole pipe. Boyles's law is originated from the ideal gas law. The compressibility factor, z, is unknown due to the humidity of the gas that are mixed with water, and an ideal gas is therefore assumed[5].

The correction of gas fraction by volume expansion were estimated by dividing the pipe into small segments, as illustrated in *Figure 12*. **Error! Reference source not found.**

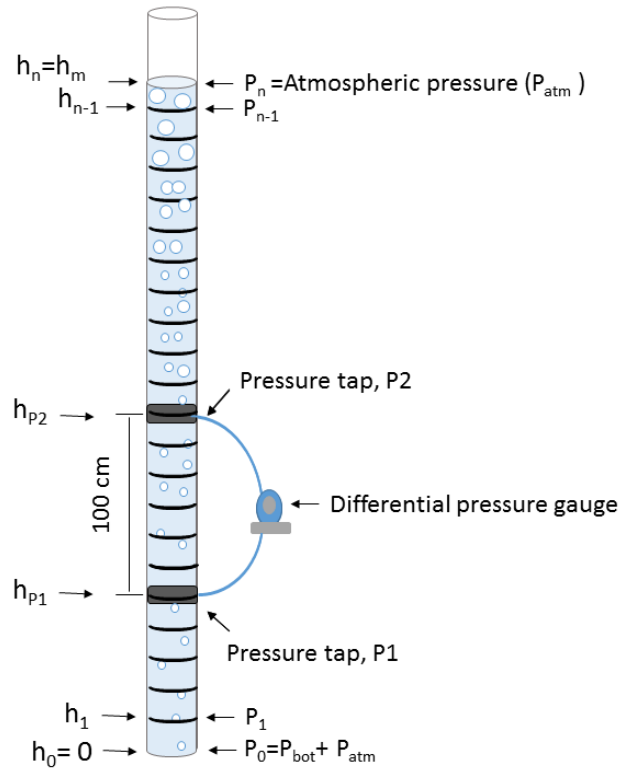


Figure 12 Estimation of gas expansion in the liquid level method

By knowing the bottom hole pressure (P_{bot}) from transmitter 1 and the height of the fluid inside the riser (h_m), an increase ratio in bubble volume can be calculated stepwise for each segment, by assuming a linear pressure drop along the pipe as a function of the height from the bottom of the riser. The linear pressure drop along the riser is found by:

$$\frac{dP}{dh} = -\frac{P_0 - P_n}{h_0 - h_n} \quad \text{Equation 4.19}$$

Where,

P_0 : Pressure at the bottom at the riser = $P_{bot} + P_{atm}$

P_n : Atmospheric pressure (P_{atm})

h_0 : height at bottom of the riser = 0

h_n : height of the mixed fluid in the riser = h_m

The pressure drop from Equation 4.19 then becomes:

$$\frac{dP}{dh} = \frac{P_{bot}}{h_m} \quad \text{Equation 4.20}$$

The pressure in each segment, i , are then found by:

$$P_i = P_0 - \left(\frac{dP}{dh} h_i \right) \quad \text{Equation 4.21}$$

Where h_i represent the distance from the bottom (h_0) in each segment i . The distance between each segment (dh) is set to 0.01m.

By using Boyle's law (Equation 4.18) the ratio between the bubble volume at each segment (V'_i) and the bubble volume at the bottom of the riser (V_0) becomes:

$$V'_i = \frac{V_i}{V_0} = \frac{P_0}{P_i} \quad \text{Equation 4.22}$$

The average in-situ bubble volume ratio then becomes:

$$\overline{V'_{in-situ}} = \frac{1}{i_b - i_a} \sum_{i=i_a}^{k=i_b} V'_i \quad \text{Equation 4.23}$$

Where i_a and i_b are the i -th number of segments at two specific heights a and b . To compare the liquid level method with the differential pressure method a and b were chosen as the height at pressure tap1 (P_1) and pressure tap2 (P_2).

The average ratio between the gas in the riser and the volume at the bottom of the riser then becomes:

$$\overline{V'_{riser}} = \frac{1}{n} \sum_{i=0}^n V'_i \quad \text{Equation 4.24}$$

Where n is the number of segments given by:

$$n = \frac{h_m - h_0}{dh} = \frac{h_m}{dh} \quad \text{Equation 4.25}$$

The gas fraction found by the liquid level method is inside the fluid in the whole riser given by Equation 4.17, and can be written as:

$$\varepsilon_{g_ave} = \left(\frac{V_g}{V_m} \right)_{riser} \quad \text{Equation 4.26}$$

By dividing the gas fraction found from the liquid level method with $\overline{V'_{riser}}$ and multiplying with $\overline{V'_{in-situ}}$, the volume expansion of gas is corrected for and in-situ gas fraction are found:

$$\varepsilon_g = \frac{\overline{V'_{in-situ}}}{\overline{V'_{riser}}} \left(\frac{V_g}{V_m} \right)_{riser} = \frac{\overline{V'_{in-situ}}}{\overline{V'_{riser}}} \varepsilon_{g_ave} \quad \text{Equation 4.27}$$

4.4.2.3 Change in rise velocity

The rise velocity for a gas bubble increases with increased bubble size, but if the bubble size becomes bigger than the diameter of the pipe and creating a Taylor bubble, the rise velocity of the gas will then decrease[2]. In the experiments performed in this thesis the standard rise velocity theory do not apply, due to interaction between several bubbles that will interfere with the velocity of the bubbles[5]. Thus, the change in rise velocity cannot be corrected for in these experiments.

4.5 Calculating the expected apparent weight of the pendulum by using Archimedes principle

As mentioned in chapter 2.1 the Archimedes' principle states that "The magnitude of the buoyant force on an object always equals the weight of the fluid displaced by the object". To compare this principle with the apparent weight measured by the force sensor the apparent weight expected by using Archimedes principle needs to be calculated. By using the apparent weight Equation 2.8 the buoyancy Equation 2.5 and the equation for mixture density Equation 4.11a relation between the expected apparent weight and gas fraction can be found by:

$$W' = F_g - \rho_{fluid} g V_{disp} = F_g - \left(\rho_g \varepsilon_g + \rho_w (1 - \varepsilon_g) \right) g V_{disp} \quad \text{Equation 4.28}$$

Where W' is apparent weight, F_g is true weight of the pendulum, ε_g is gas fraction, ρ_g and ρ_w is the density of gas and water, respectively. In the experiments, air is used as the gas. Standard conditions for the density of air and water is assumed ($\rho_g = \rho_{air} = 1.3 \text{ kg/m}^3$ [2], $\rho_w = 1000 \text{ kg/m}^3$ [2]). The volume displaced is found by the of the bob (V_{bob}) as described in section 4.1

Equation 4.28 then becomes:

$$W' = F_g - \rho_w g V_{bob} + (\rho_w \varepsilon_{air} - \rho_{air} \varepsilon_{air}) g V_{bob} \quad \text{Equation 4.29}$$

After having explained the analytical methods, the next chapter will present and discuss the results from the experiments

5. Results and discussion

In the results and discussion part the methods described in Chapter 4 will be used to analyze the experimental data from the experimental setups described in Chapter 3.

The results and discussion part of the thesis is divided into two parts. The first part will contain the development-process. By describing and discussing the modifications that were made to the experimental setup as a result of analyzes of the feasibility setup experiments. This part also includes changes necessary due to problems that occurred when converting from the small-scale feasibility setup to the larger-scale more extensive main experimental setup.

The second part is an analysis of the adequacy of the experimental setup in relation to the objective of the study. In this part the experimental data from the differential pressure gauge and the liquid level measurements of the fluid in the pipe is compared with data gathered with the new proposed method.

5.1 Modifications in experimental setup

5.1.1 Feasibility experiments

To develop an adequate experimental setup- some trial and error proved necessary. Before running the experiments on a big scale, a simple smaller scale feasibility test was built to see if using buoyancy to measure gas fraction in a pipe is possible, to test the equipment and to see if any adjustments to the setup, pendulum and fluid used were necessary. The development-process for the feasibility setup will be explained in this section.

5.1.1.1 Pendulum design

The most demanding and challenging task was to find a pendulum that ensured reliable results. When designing the pendulum, several components must be considered. Shape, size, density of the bob and type of string will have an effect on the experimental result. Key requirements for a good designed pendulum are good passage for the fluid and gas inside the pipe, no movement of the bob, negligible friction and capillary forces against the wall and a volume big enough to capture the changes in buoyancy as the gas fraction changes. It is also important that the forces

acting on the pendulum never exceed the force sensors' capacity or make the pendulum weightless.

The bob

The first bob used in the feasibility setup was a 300 gram led fishing weight. The fishing weight was chosen because of its round and smooth shape. This is desirable because it does not trap any gas bubbles and the fluid gets a smooth passage when flowing past the bob. The specifications and a picture of the fishing weight is found in *Table 2* and *Figure 13*.

Name of bob	Fishing weight
Weight in air (F_g) [N]	2.815
Weight in water (W') [N]	2.501
Volume (V_{bob}) [mL]	32
Length [cm]	8
Diameter max [cm]	3,8

Table 2 Specifications of the fishing weight



Figure 13 Fishing weight

The fishing weight could only be tested with the PASCO force sensors. The reason for this is that the fishing weight is too heavy for the Mark-10 force sensor, which reaches maximum force at 2.5N (specifications of the force sensors can be found in Appendix A). To be able to use the more accurate Mark-10 force sensor, the weight of the pendulum therefore had to be reduced. To recall from Chapter 2.1, the buoyancy depends on the displaced volume and the density of the fluid. When decreasing the density of the fluid by injecting gas, the buoyancy will decrease. The decrease in buoyancy will depend on the volume of the displaced fluid. This means that a change in buoyancy is dependent on the displaced volume, which is the volume of the bob. It is therefore favorable to have a bob with a big volume. Consequently, if the volume of the bob is not to be reduced, the material of the new bob must be lower than the density of the fishing weight.

The bob chosen was a cylinder-shaped bob made in acrylic glass. The specifications and a picture of the Acrylic cylinder is found in *Table 3* *Figure 14 Acrylic glass cylinder* and *Figure 14*. The Acrylic glass was chosen because it has a density which is slightly above the density

of water. A denser material than water makes the pendulum sink. A material close to the density of water allows the biggest volume possible without overloading the Mark-10 force sensor.

Name of bob	Acrylic cylinder
Weight in air (F_g) [N]	0.598
Weight in water (W') [N]	0.0873
Volume (V_{bob}) [mL]	52.1
Length [cm]	10.6
Diameter [cm]	2.5

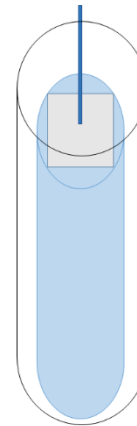


Table 3 Specifications of the Acrylic cylinder

Figure 14 Acrylic glass cylinder

When comparing the results between the fishing weight and the acrylic cylinder it was noticed that the shape of the bob had a big impact on the flow. The cylinder shape disturbed the flow more than the rounded shape of the fishing weight. The flat bottom of the cylinder captured the gas and created slugging in the system. This led to considerable oscillations in the apparent weight that was measured by the force sensor. This can be seen by looking at the high standard deviation values in *Figure 16*. The figure shows the average change in apparent weight as a function of gas fraction for the bobs tested during the feasibility experiments. The red graph shows the result from the Acrylic cylinder. At high gas injection rates, the oscillations started to exceed the force sensor's capacity. As a solution, the bob was reduced by coning the bottom and top of the cylinder to reduce gas caption and to lower the oscillations. This bob will be called the "Coned acrylic cylinder".

Name of bob	Acrylic cylinder
Weight in air (F_g) [N]	0.296
Weight in water (W') [N]	0.049
Volume (V_{bob}) [mL]	25.2
Length [cm]	7.5
Diameter max [cm]	2.5

Table 4 Specifications of the Acrylic Cylinder



Figure 15 The coned Acrylic cylinder

A picture of the coned acrylic glass cylinder is shown in Figure 15. By coning the top and bottom of the cylinder, the flowage passage of the fluid improved and the standard deviation in average apparent weight was highly reduced.

Figure 16 shows the average change in apparent weight as a function of gas fraction for the different bobs tested during the feasibility experiments. The graphs in Figure 16 are found by using the method for experimental data processing presented in Chapter 4.2 and by the liquid level method described in Chapter 4.4.2. The blue, green and red curves show the average change in apparent weight for the Coned Acrylic Cylinder, the Fishing Weight and the Acrylic Cylinder, respectively.

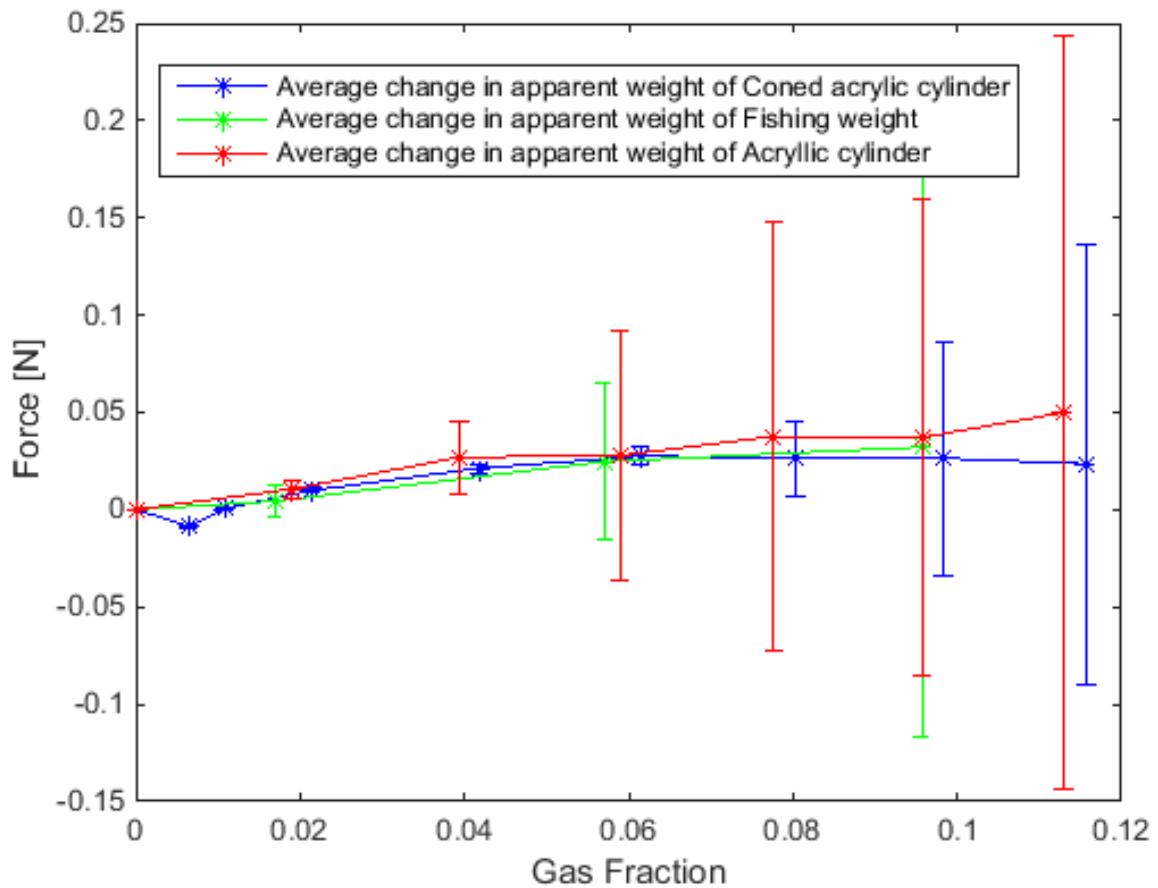


Figure 16 Comparison of the change in average weight as a function of gas fraction of the bobs tested in the feasibility experiments.

Choosing the string

The string must be strong enough to hold the apparent weight of the bob during the experiments, and it should be easily straightened, to avoid the string from coiling. The first string tested was

a 0.7 mm fishing line with a maximum strength of 23 kg. No problems were detected when using the 0.7 mm fishing line together with the fishing weight. The force that the string was exposed to was large enough to straighten out the string. For the acrylic glass bobs, the force between the bob and the force sensor was not sufficient to straighten the 0.7mm fishing line. The string started to coil, which had an impact on the experimental data result. To avoid the string from coiling, a sewing thread was used together with the Coned acrylic bob.

5.1.1.2 Type of Force Sensor

The different force sensors tested was a PASCO 5N Load Cell and a Mark-10 MR03-05 Force Sensor. Specifications for the two force sensors can be found in the Appendix. In the force sensor, the quality desired is firstly high accuracy. The precision must be high enough to capture the small changes in force that are acting on the system. It is also important that the apparent weight of the pendulum don't exceed the capacity of the force sensor. Both criteria became a constrain in the experiments. As previously mentioned the fishing weight exceeded the capacity of the Mark-10 force sensor.

Figure 17 shows the average increase in apparent weight of the coned acrylic bob, with standard deviations, as a function of gas fraction for two experiments in the feasibility phase. The first experiment is executed with a PASCO 5N Load Cell force sensor. The second experiment is executed with a Mark-10 force sensor.

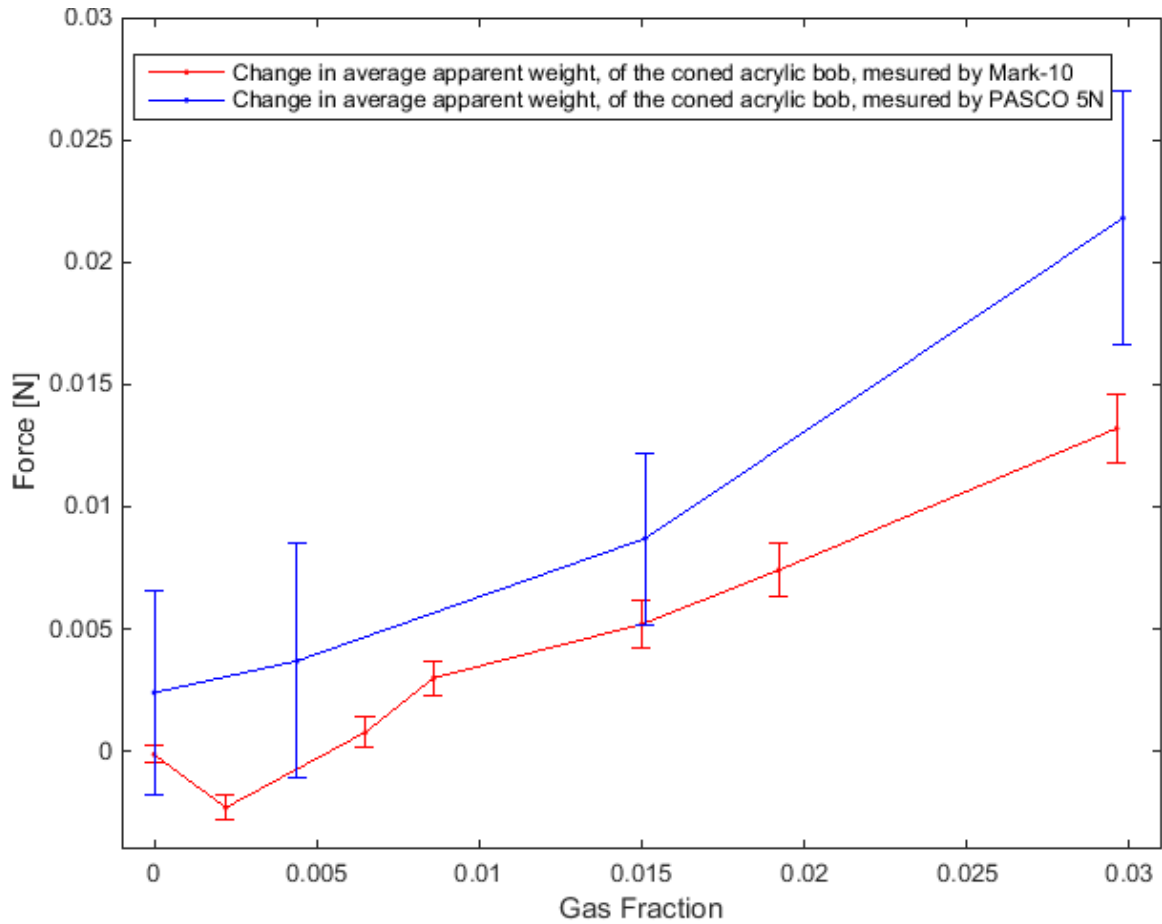


Figure 17 Comparison of the mark-10 force sensor and the PASCO 5N load cell

As described in Chapter 3.1.2, before starting the experiments in the feasibility phase, the force sensor was tared when the pendulum was submerged in pure water. Which means that the average value for apparent weight when no gas is injected should be zero. The result from the comparison in *Figure 17* shows that the average value measured by the PASCO 5N sensor at no gas injection is considerably higher than zero, which affected the rest of the measurements. PASCO 5N load cell is therefore concluded not accurate enough for this experiment. The PASCO 5N load cell will therefore not be used further in the experiments. Consequently, this decision also excluded using the Fishing weight.

In the graph from the Mark-10 force sensor in *Figure 17* the apparent weight of the pendulum decreased when very low injection rates (low gas fractions) was injected. This contradict the theory of Archimedes principle. A suggestion for this behavior will be introduced in section 5.1.3.

5.1.1.3 Type of fluid

Two fluids were tested in the feasibility experiments; water and a PAC4 solution. PAC4 is a solution consisting of a mixture with 1000 gram of water per 4 gram of polyaluminum chloride.

By adding polyaluminum chloride to water the viscosity will increase. The PAC4 solution were tested to see if the movement of the pendulum could be reduced, by using a more viscous fluid. Reduction of movement is desired to reduce the oscillations in the apparent weight of the pendulum. *Figure 18* Shows a comparison between the average change in apparent weight as a function of gas fraction for the PAC4 solution and water. The graph for the PAC4 solution shows a much larger standard deviation compared to the standard deviation for water, which means that the oscillations were increased and not reduced.

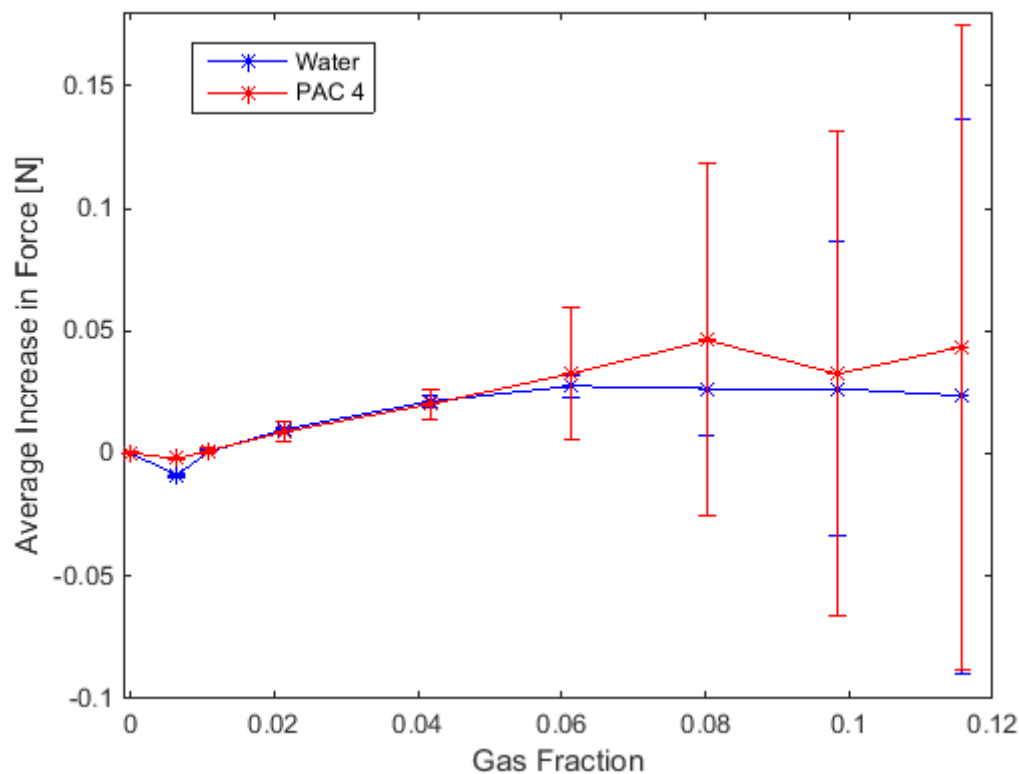


Figure 18 Comparison in average apparent weight of the pendulum for PAC4 solution and water

The reason for why an increase in viscosity increased the oscillations of the pendulum, can be explained by looking at what happens to the air bubbles in the more viscous liquid compared to water. Figure 19 and Figure 20 show pictures from an experiment with a PAC4 solution to the left and an experiment with water to the right. In Figure 19 the injection rate corresponds to a gas fraction of 0.0214. By increasing the viscosity, the gas injector was no longer able to disperse the air bobbles evenly. In Figure 20 the injection rate corresponds to a gas fraction of 0.0984. In the more viscous fluid the bubbles will merge into Taylor bubbles at lower gas fractions, which is illustrated by the drawn red contour lines around the bubbles in Figure 20. The blue contour lines capture the Coned Acrylic Cylinder. When slugging appears, the

pendulum will alternate between being fully submerged in the fluid and being inside a bubble. This will create big oscillations in the apparent weight. It is preferred to avoid slugging due to further analysis of the data. Due to the low distribution of bubbles and the early slugging, the PAC4 will not be used in the further experiments.

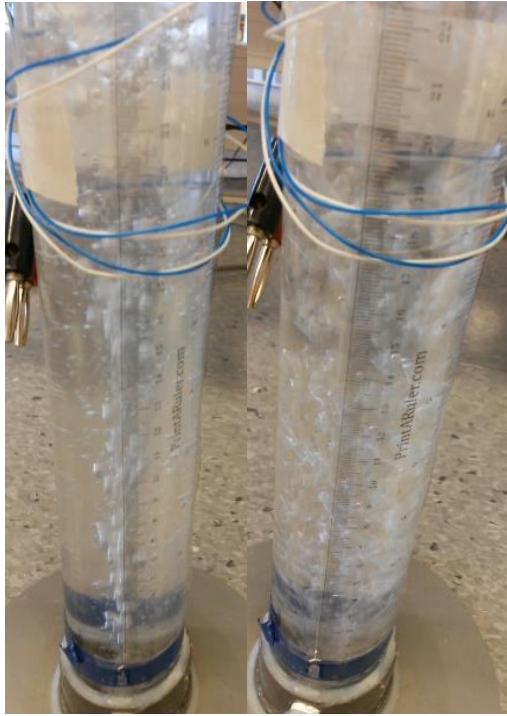


Figure 19 Comparison between the gas bubbles inside a PAC4 solution (left) and in water (right) at a gas fraction of 0.0214.

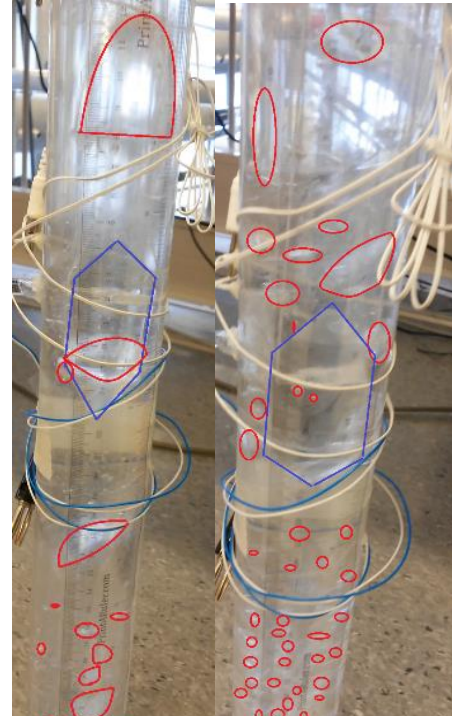


Figure 20 Comparison between the gas bubbles inside a PAC4 solution (left) and in water (right) at a gas fraction of 0.0984.

5.1.2 Converting from the feasibility test to the main experiment setup

The second part of the development-process was to convert the knowledge from the feasibility setup into the larger-scale experimental setup. From the tests in the feasibility setup, the following equipment used in the larger-scale more extensive experimental setup:

- Fluid: water
- Pendulum: Coned acrylic cylinder (bob) connected to a sowing thread (string)
- Force sensor: Mark-10 MR03-05force sensor

The rest of the setup are described in Chapter 3.

When using the larger main setup some problems occurred:

1. The sowing thread was sticking to the pipe
2. The coned acrylic cylinder becomes weightless at high injection rates
3. The dispersion of bubbles was lower for the gas injector in the existing flow loop system than the gas injector used in the feasibility setup

Due to these problems more changes were necessary and will be discussed in the following sections.

5.1.2.1 String sticking to the pipe

The sowing thread worked perfectly at the feasibility setup, but when using the longer flow loop set up, the string started to stick to the wall in the area between water and air. It is likely to believe that this is caused by capillary forces between a wet sowing thread and a humid pipe. As the sowing thread was sticking to the pipe, it was difficult to hose the bob down to the differential pressure taps. In order to fix this problem, the string was replaced with a 0.04 mm Suffix nanobraid string, with a maximum strength of 2.8 kg (27.5N).

5.1.2.2 Weightlessness of the coned acrylic bob

When using the flow loop setup, the oscillations of the apparent weight of the pendulum increased considerably and weightlessness of the Coned acrylic glass bob was noticed after analyzing the data. Figure 23 shows the average increase in apparent weight of the pendulum as a function of gas fraction. The blue graph shows the results from the feasibility setup and the red graph shows the results from an experiment with the flow loop setup. The reason for this change was found to have connection to that two different gas injectors were used in the feasibility and the flow loop experiment, because they affected the flow differently. In the feasibility setup a gas sparger with a sintered filter cartridge injector was used. In the flow loop experiment a 1/16 inch Swagelok nipple was used as an injector. The flow pattern for the two gas injectors is shown in Figure 21 and below Figure 22.



Figure 21- Flow pattern between the two pressure taps at 0.2; 0.5; 1.0; 1.5; 2.0; 2.5; 3.0 SPLM of gas (air) for the swagelok nipple 1/16 inch injector [8]



Figure 22 Flow pattern between the two pressure taps at 0.2; 0.5; 1.0; 1.5; 2.0; 2.5; 3.0 SPLM of gas (air) for the gas sparger with sintered filter cartridge injector

The difference between the injectors had a great impact on the gas dispersion in the flow, as can be seen in Figure 21 and aboveFigure 22. The dispersion of gas bubbles when using the 1/16 inch Swagelok was highly rescued and caused an increase in oscillations of the apparent weight. The oscillations are presented as a standard deviation of the average increase in the

apparent weight in *Figure 23*. The gas fractions used in the graphs in *Figure 23* was found by using the liquid level method and the differential pressure method presented in chapter 4.4.

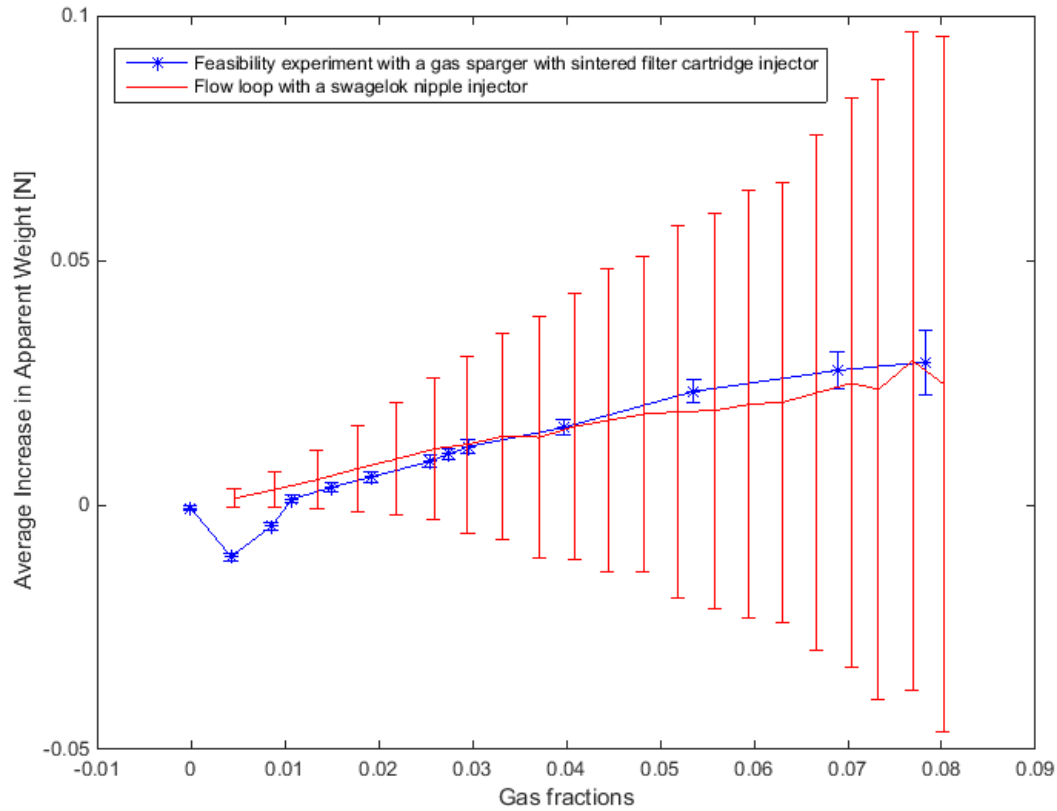


Figure 23 Comparison of average increase in apparent weight of the pendulum as a function of gas fraction for two different gas injectors

Figure 24 shows the apparent weight of the pendulum as a function of time for two different gas injection rates, 0.8 and 5 SLPM executed with the main experiment. At a gas injection rate of 5 SLPM the apparent weight was measured to be zero. This indicates that the pendulum is weightless, which means that after a certain injection rate, the forces action upwards on the pendulum starts to exceed the forces acting downwards on the pendulum. The apparent weight measured from the pendulum was found to reach weightlessness with gas injection rates down to as low at 0.6-0.8 SLPM. Consequently, all data measured and analyzed for gas injections rates above 0.6 SLPM must be discarded.

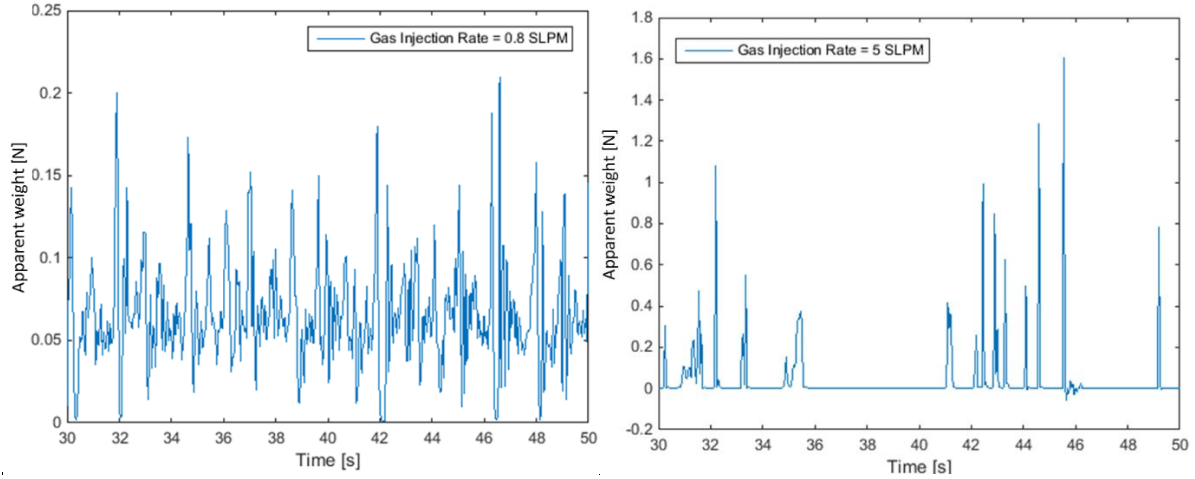


Figure 24 Pendulum becomes weightless as injection rate increases

To fix the weightlessness and the increase in oscillations in apparent weight, two changes were done to the flow loop setup. The 1/16 inch Swagelok nipple was exchanged with the gas sparger with sintered filter cartridge injector used in the feasibility experiments, and a new bob was designed.

To be certain that the pendulum does not become weightless the forces working downward on the pendulum may be increased and the forces working upward on the pendulum may be reduced. A known downward working force on the pendulum is the gravity force. This can be increased by increasing the volume and the density of the bob. Drag force works on the pendulum from the same direction as the flow and will therefore contribute to decrease the apparent weight of the pendulum. Drag force are given by Equation 5.1 [9].

$$F_d = C_D \frac{\pi d^2}{8} \rho U^2 \quad \text{Equation 5.1}$$

Where C_D is the drag coefficient, d is the diameter of the bob, ρ is the density of the fluid and U is the velocity of the fluid.

The drag force can be reduced by reducing the diameter of the pendulum. The volume of the bob is equivalent with the buoyancy and should therefore not be reduced. The solution was to increase the density, reduce the diameter and increase the length of the bob. The coned acrylic cylinder bob was therefore exchanged with a stainless-steel bar. To prevent pendulous movements of the steel bar, small pipes were glued to the side of the of the steel bar. The

specifications and a picture of the Acrylic cylinder are presented in Table 5Table 3Figure 14 Acrylic glass cylinder and in Figure 25, respectively.

Name of bob	Steel bar
Weight in air (F_g) [N]	1.044
Weight in water (W') [N]	0.750
Volume (V_{bob}) [mL]	30
Length [cm]	85
Diameter (excluding pipes) [cm]	0.5

Table 5 Specifications of the Steel bar



No indications of weightlessness were found at high injection rates and the oscillations of the apparent weight was considerably reduced, when using the steel bar bob and the gas sparger with sintered filter cartridge injector.

The equipment used for the final experiments are described in Chapter 3.2. Where water is used as the fluid, the Mark-10 MR03-05 is used as a force sensor, the pendulum used is the steel bar bob with the 0.04 mm Sufix nanobraid string and the gas injector is the Gas sparger with sintered filter cartridge. Three experiments where run with this final setup. The results are analyzed and discussed in Chapter **Error! Reference source not found..**

In section 5.1.1.2 it was mentioned the at very low injection rates the apparent weight of the pendulum decreased when injecting gas. Before analyzing the three final experiments a suggestion for why the weight of the pendulum is decreasing will be introduced.

5.1.3 Bubbles attaching to the bob

When using the gas sparger with a sintered filter cartridge for gas injection at very low flow rates (gas fractions less than 0.006 and injection rate less than 0.05 SLPM), the average change in apparent force of the pendulum is negative. This is illustrated by the graph of the change in apparent weight of the pendulum measured by the Mark-10 force sensor in *Figure 17*. The trend was noticed to be associated with very small bubbles that get attached to the surface of the bob, as shown in Figure 26. The bubbles attached to the bob contributes to push the bob upwards

leading to a lower apparent weight measured by the force sensor. In stagnant liquids, the bobbles will attach if the difference between gravitational forces and buoyancy forces are lower than the adhesion force[10]. This means that the size of the bobbles has a big effect on bubbles attaching the pendulum. The 1/16 inch Swagelok nipple injector fist used in the flow loop released much bigger bubbles than the gas sparger with sintered filter cartridge, which may explain why this is not a trend detected when using the 1/16 inch Swagelok nipple injector. In the final experiments the lowest gas injection rate used was 0.01 where the bubbles did not attach to the bob.

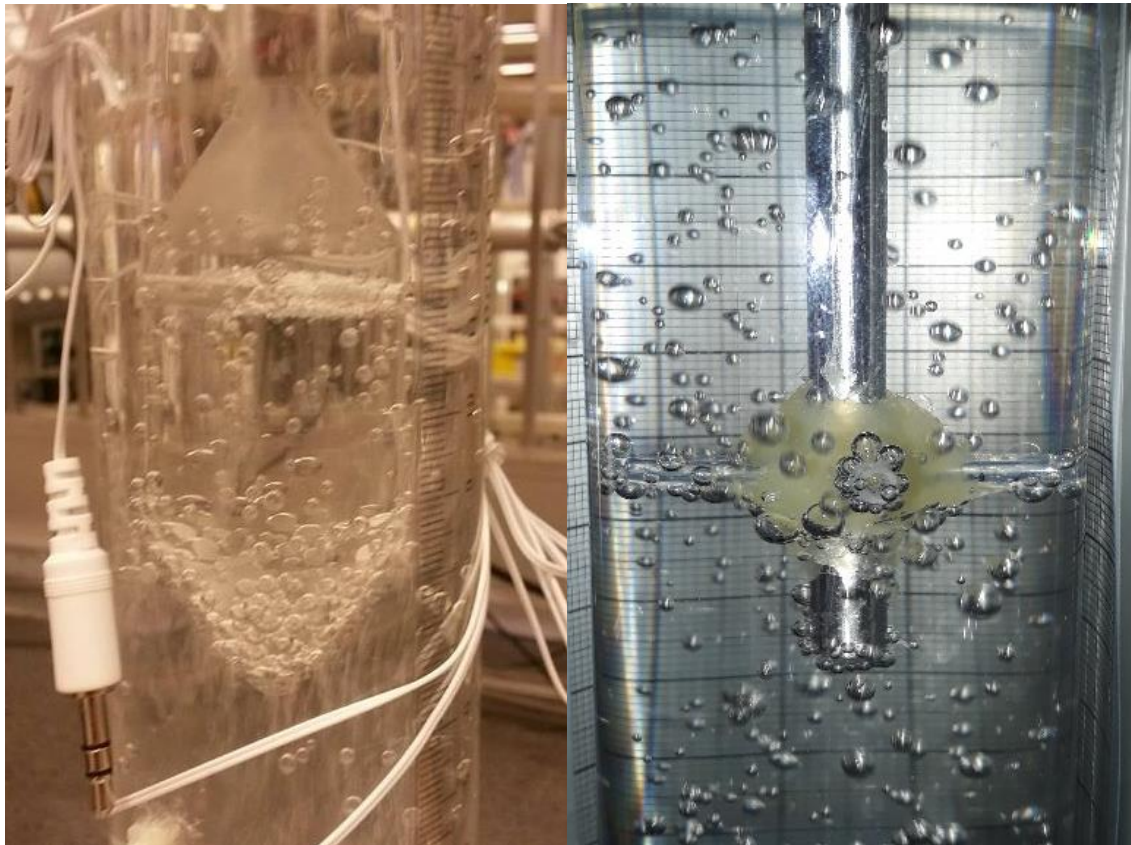


Figure 26 Bobbles attaching on the bob.

5.2 Analysis of the results from the final experiments

In this section the three final experiments will be analyzed. The final result of the experimental setup are given at the end of Chapter 5.1.2. The input values in LabVIEW used to run the three final experiments can be found in *Table 1*.

The data gathered in the final experiments (experiment 1) from the force gauge, differential pressure gauge and liquid level measurement are presented in Figure 27, Figure 28 and Figure 29. Figure 27 shows a plot of the apparent weight of the pendulum measured by the force sensor as a function of gas injection rate. Figure 28 shows a plot of the differential pressure measured by the differential pressure gauge as a function of gas injection rate. For the force and differential pressure the experimental data processing method described in Chapter 4.2 is used to create the two plots. In Figure 27 and Figure 28 the experimental data processing method described in Chapter 4.2 is used to create the two plots. Figure 29 is the gas fractions found from the Liquid Level Method, described in Chapter 4.4.2, as a function of gas injection rate.

5.2.1 Apparent Weight of the Pendulum

As mentioned Figure 27 shows a plot of the apparent weight of the pendulum measured by the force sensor as a function of gas injection rate. This figure shows that as the injection rate increases, the apparent weight (W') of the pendulum increases. This is expected since an increase in the gas injection rate, increases the gas fraction in the riser, and therefore reduces the buoyancy force acting on the pendulum. Which can be seen from Equation 4.29. The relation between the injection rate and the gas fraction will be analyzed in section 5.2.3. To better understand the behavior of this curve, further analyses are necessary. Also noticed in this figure is that as the gas injection increases, the standard deviations in the plot increases, which means that the oscillations in the force measured also increases.

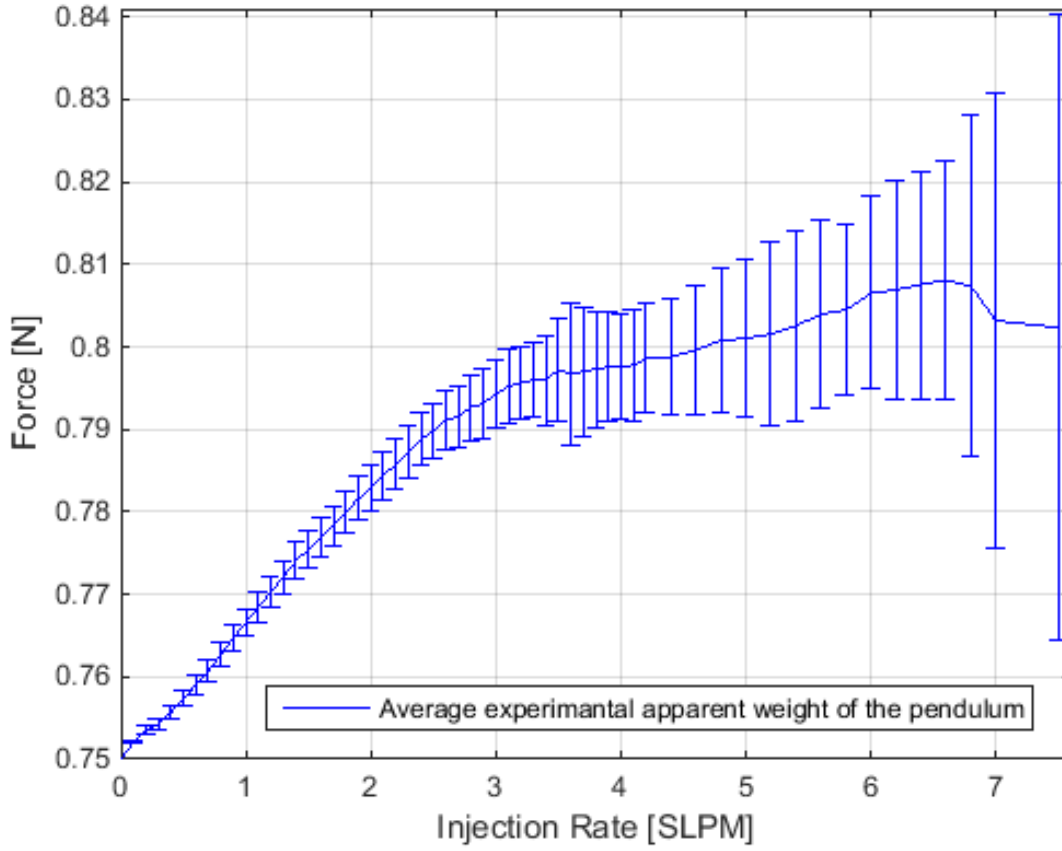


Figure 27 Average experimental apparent weight of the pendulum measured by the force sensor as a function of injection rate

5.2.2 Differential Pressure Measurement

As mentined Figure 28 shows a plot of the differential pressure measured by the differential pressure gauge as as a function of gas injection rate. From this figure it is observed that as the injection rate increases the differential pressure becomes larger. Since an increase in gas injection rate increases the gas fraction inside the pipe the behavior of the plot in Figure 28 can be described by looking at the differential pressure equation (Equation 4.14) derived in Chapter 4.3:

$$p_{diff} = (\varepsilon_g \rho_w - \rho_g \varepsilon_g)g - \Delta p_f \quad \text{Equation 4.14}$$

Since the density of water (ρ_w) allways will be higher that the density of gas (ρ_w) and increase in gas fraction (ε_g) will increase the differential pressure (p_{dif}). The differential pressure is also dependant on the frictinal pressure drop (Δp_f) in the pipe. The frictional differential pressure

drop will always be positive in the direction of flow an increase in frictional pressure drop will decrease the differential pressure. The increase in differential pressure with injection rate shown in Figure 28 indicates that the differential pressure is mainly due to a change in gas fraction. The effect of frictional pressure drop in the differential pressure will be discussed the comparison between the liquid level- and differential pressure method of finding gas fraction in section 5.2.4.

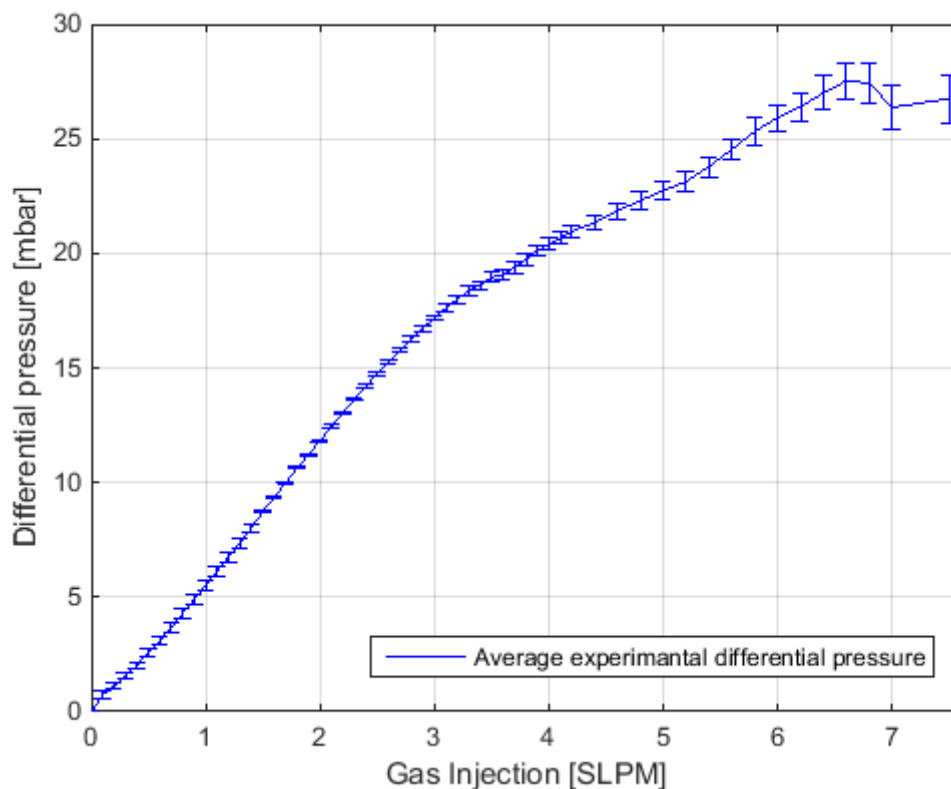


Figure 28 Differential pressure as a function of gas injection rate

5.2.3 Gas Fractions from the Liquid Level Method

Figure 29 shows how the gas fraction increases with increasing injection rate by using the liquid level method. In the figure, there are two plots. The red curve is created by using the liquid level method without correcting for gas expansion. The green graph shows the same when correcting for gas expansion.

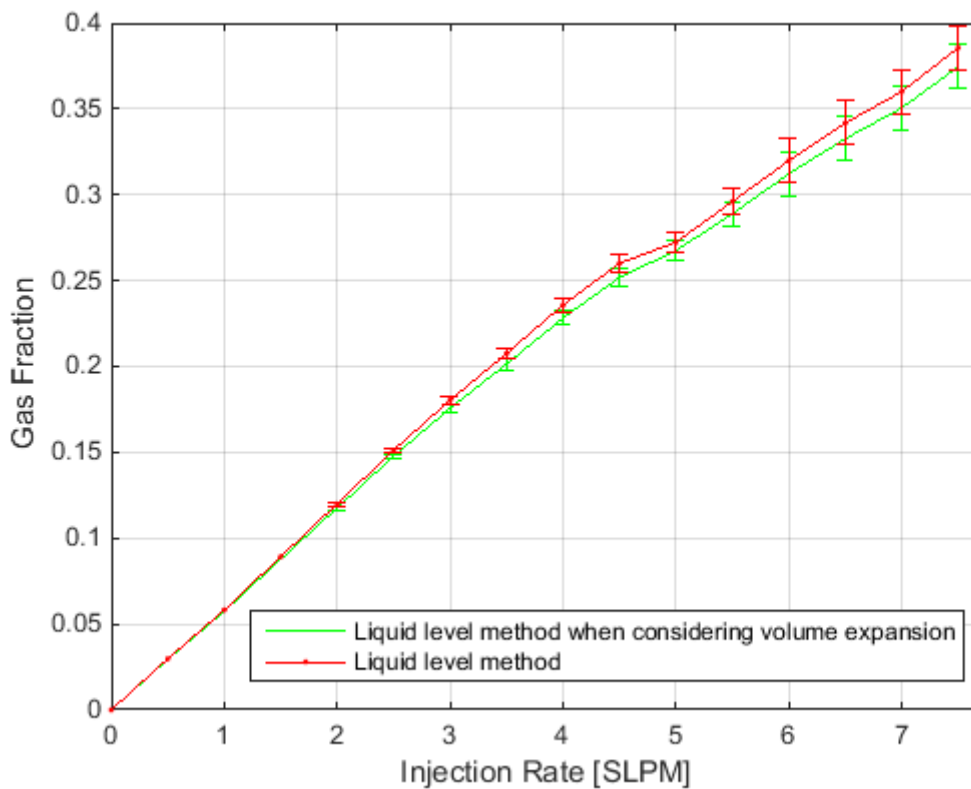


Figure 29 Gas fraction measured by the Liquid Level Method, with and without correcting for gas expansion

The difference found between the Liquid Level Method without correcting for gas expansion and the method when correcting for gas expansion is small. But a slight overestimation of gas fraction was noticed when the expansion is not accounted for, especially when the gas injection increases. For further analysis, the liquid level method with correction for gas expansion will be used.

5.2.4 Comparison between the Liquid Level - and the Differential Pressure Method for finding gas fractions

A comparison between measuring the gas fraction as a function of the injection rate by the use of the Liquid Level Method and the use of the Differential Pressure Method is shown in Figure 30. The blue curve shows the differential pressure data from Figure 28 converted to gas fractions by the Differential Pressure Method described in Chapter 4.4.1. The green curve is green curve (Liquid Level Method when considering gas expansion) from Figure 29.

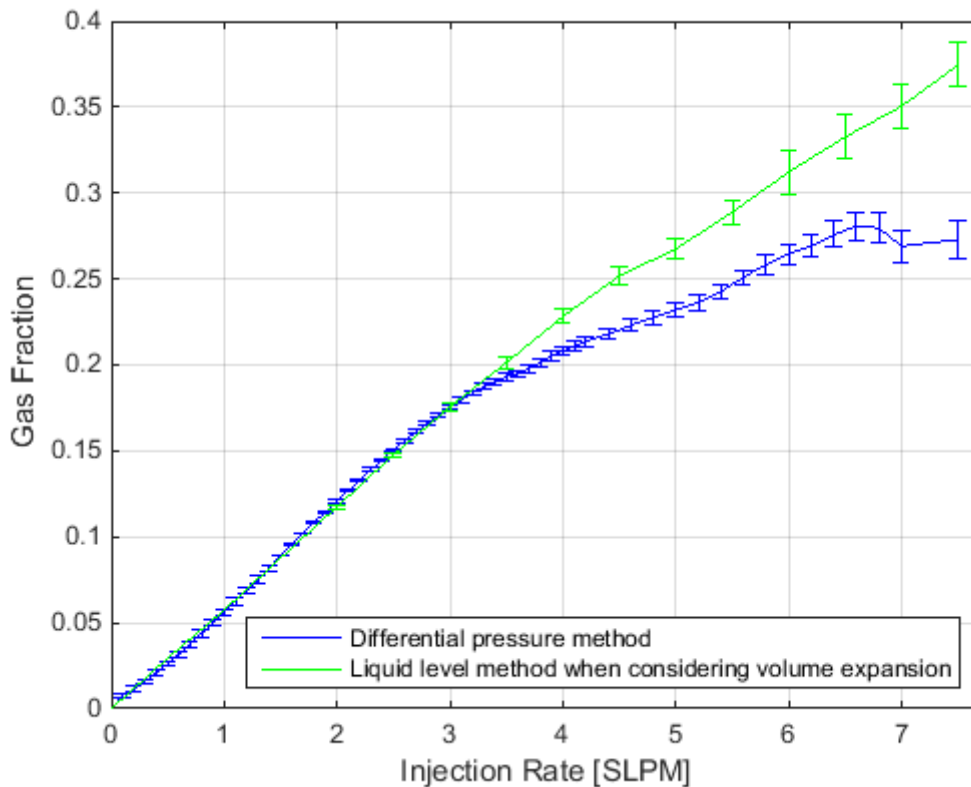


Figure 30 Comparison between the liquid level method and the differential pressure method

Figure 30 shows that the result when using the Liquid Level- and the Differential Pressure Method is the same up to a gas injection rate above 3 SLPM. Then the Differential Pressure Method shows a lower gas fraction for increasing injection rates than the Liquid Level Method. This may be explained by a frictional pressure drop in the pipe. When the differential pressure data was converted into gas fractions, the frictional pressure gradient and the acceleration pressure gradient were assumed negligible. See Chapter 4.4.1. As previously mentioned, the frictional pressure drop may influence the system. When assuming a negligible frictional pressure gradient, the gas fractions calculated by the use of the Differential Pressure Method may have been over underestimated. From Equation 4.15 in chapter 4.4.1, we can see that by assuming that the frictional pressure drop is equal to zero, the gas fraction will be underestimated, if the differential pressure is not negligible. From the comparison between the liquid level and differential pressure method, we can see that it is no longer only the hydrostatical pressure (effected by the change in gas fraction) that influence the differential pressure. Which means that the differential pressure method of measuring gas fraction cannot be used above

injection rates of 3.0 SLPM in these experiments, since we do not know the frictional pressure drop.

5.2.5 Gas fractions at different injection rates

From the data acquired from the Liquid Level Method for gas injection rates above 3.0 SLPM, a third order polynomial trend line was made in excel to extrapolate the gas fractions for the injection rates where the Liquid Level Method was not used. The trend line with the extrapolation equation can be seen in Figure 31.

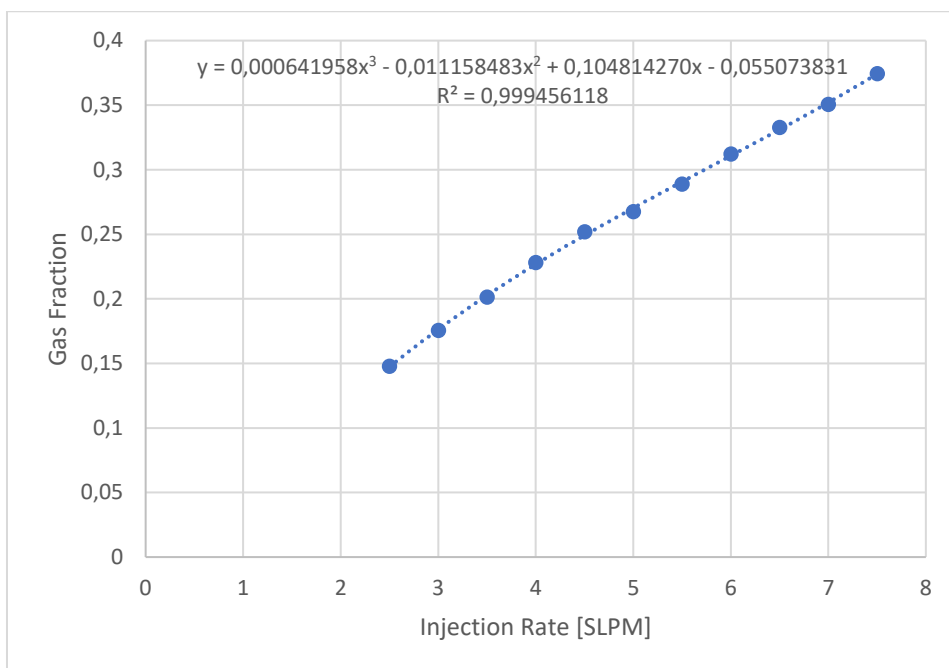


Figure 31 extrapolation of the gas fraction found by the liquid level method

The gas fraction calculated with the Differential Pressure Method below 3 SLPM and the values extrapolated from the liquid level method above 3 SLPM as a function of injection rate are presented in Figure 32. Figure 32 now represent the gas fraction between the two pressure taps for each gas injection rate used for the experiments for further analysis.

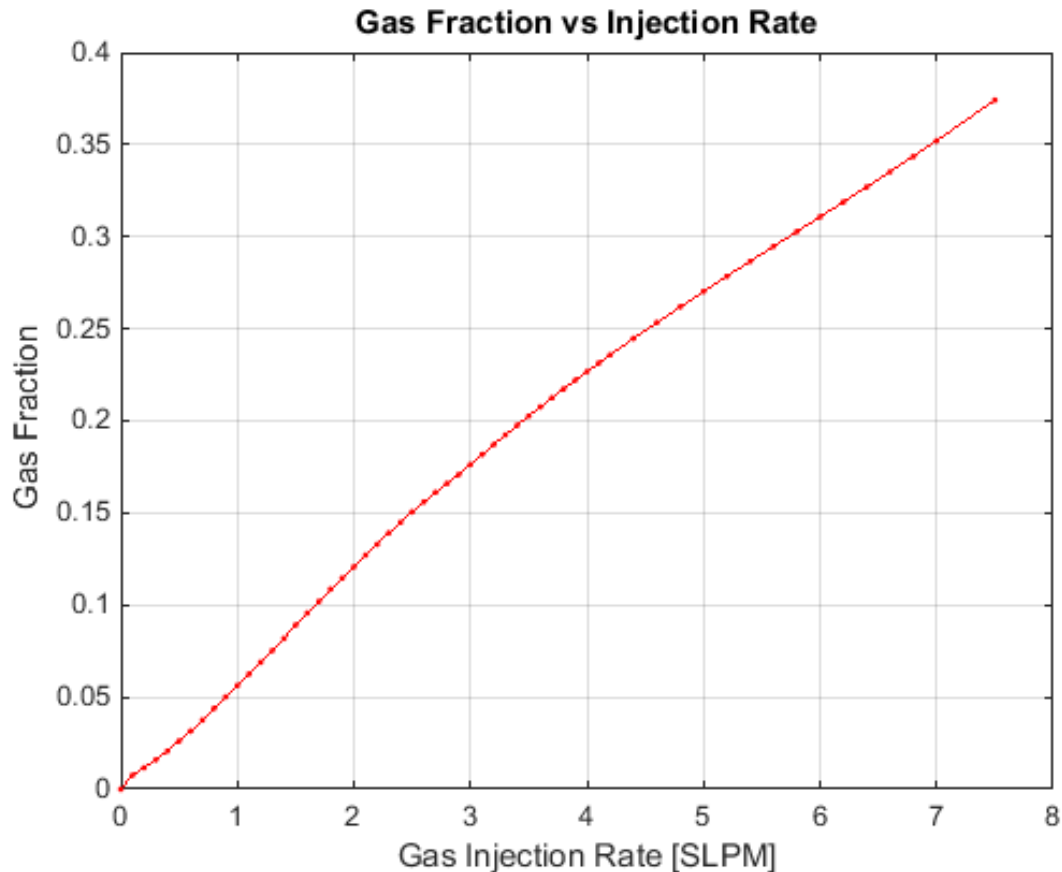


Figure 32 Gas fraction in the pipe as a function of gas injection rate

5.2.6 Can a buoyancy sensor be used to measure gas fraction in a gas-liquid flow?

5.2.6.1 Calculating the gas fraction from buoyancy

As previously mentioned in chapter 2.1, the Archimedes' principle states that "The magnitude of the buoyant force on an object always equals the weight of the fluid displaced by the object". This principle is true if the fluid is stagnant and homogeneous. However, our system is neither stagnant nor homogenous. Archimedes' principle may therefore not be true in the experimental case. To compare this principle with the data from the force sensor the expected apparent weight by using Archimedes principle needs to be calculated. In chapter 4.5 an equation for the expected apparent weight as a function of gas fraction, by use of Archimedes principle, was derived (Equation 4.29). The known parameters for the experiments are found in Chapter 4.1 and Chapter 5.1.1.1, and are presented in *Table 6*

F_g [N]	V_{bob} [m ³]	g [m/s ²]	ρ_w [kg/m ³]	ρ_{air} [kg/m ³]
1.044	$3 \cdot 10^{-5}$	9.81	1000	1.3 [2]

Table 6 Input values

By inserting the known values from Table 6 into the **Error! Reference source not found.**, the relation between expected apparent weight of the pendulum and gas fraction of air in the fluid then becomes:

$$W' = 0.750N + (2.94 \cdot 10^{-4} \cdot (10^3 \varepsilon_{air} - \varepsilon_{air}))N \quad \text{Equation 5.2}$$

The relation between expected apparent weight of the pendulum and gas fraction are plotted in Figure 33 and compared with the apparent weight of the pendulum measured during the experiment as a function of gas fraction. The gas fraction used are the gas fractions found for each injection rate plotted in Figure 32.

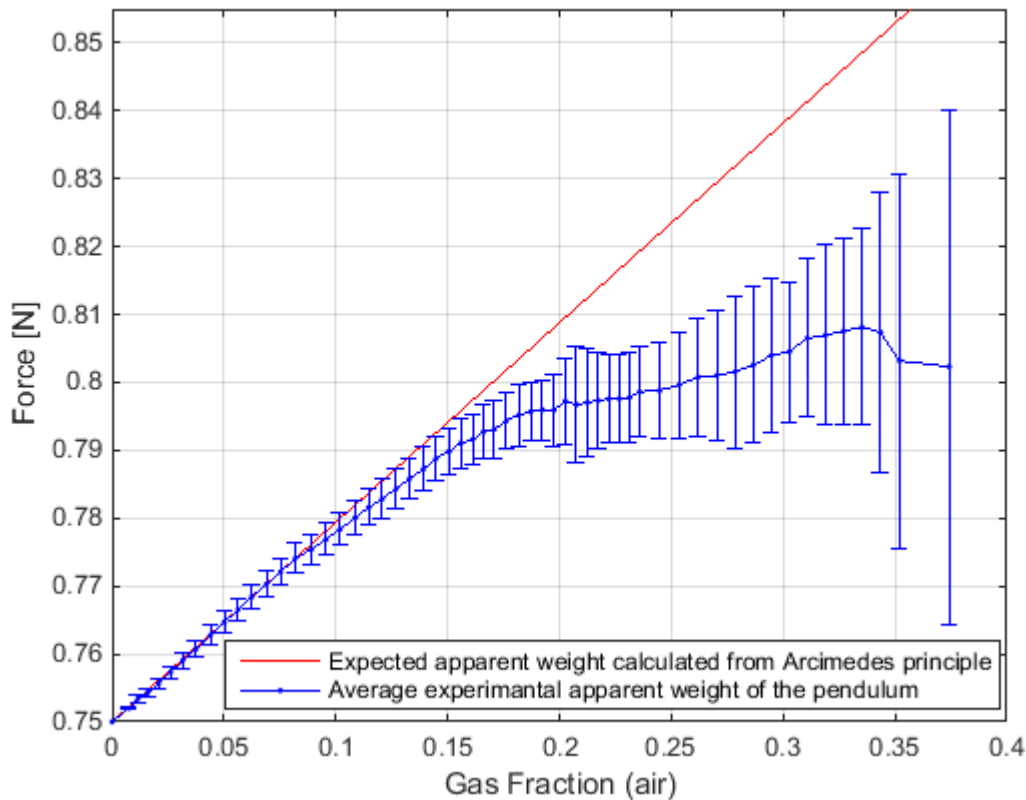


Figure 33 Expected apparent weight vs average experimental force at different gas fractions.

The comparison in Figure 33 shows that the apparent weight calculated from Archimedes' principle and the average apparent weight of the pendulum measured by the force sensor give similar results up to a gas fraction of 0.0818. A gas fraction of 0.0818 corresponds to a gas

injection rate of 1.4 SLPM. This result indicates that for this specific system, Archimedes' principle can be used to find the gas fraction in a gas-liquid flow at injection rates below 1.4 SLPM. At injection rates above 1.4 SLPM, the Archimedes' principle is no longer valid, for this specific system.

To have a better understanding of the apparent force of the pendulum measured by the force sensor a comparison with the experimental data measured by differential pressure gauge. From the comparison between the Liquid Level Method and the Differential Pressure Method for finding the gas fraction in the system, it was found that frictional pressure drop affected the differential pressure. Since Archimedes' principle is for a stagnant fluid, it only account for hydrostatic pressure drop and does not account for friction pressure loss. Equation 2.2 from Chapter 2.1 states that the buoyant force is dependent on the difference between the pressure on top and on the bottom of the pendulum, and therefore dependent on the pressure gradients presented in Chapter 2.4. The buoyancy in a moving system will therefore be dependent on all three of the pressure gradients. The trend of the data from the differential pressure gauge in *Figure 28* and the apparent weight of the pendulum measured by the force gauge from *Figure 27* are therefore compared in *Figure 34*. The differential pressure, as a function of the gas injection rate, is presented in the blue curve, and has the differential pressure values on the y-axis on the left-hand side. The experimental force as a function of gas injection rates are presented in the red curve, and has the force values on the y-axis on the right-hand side.

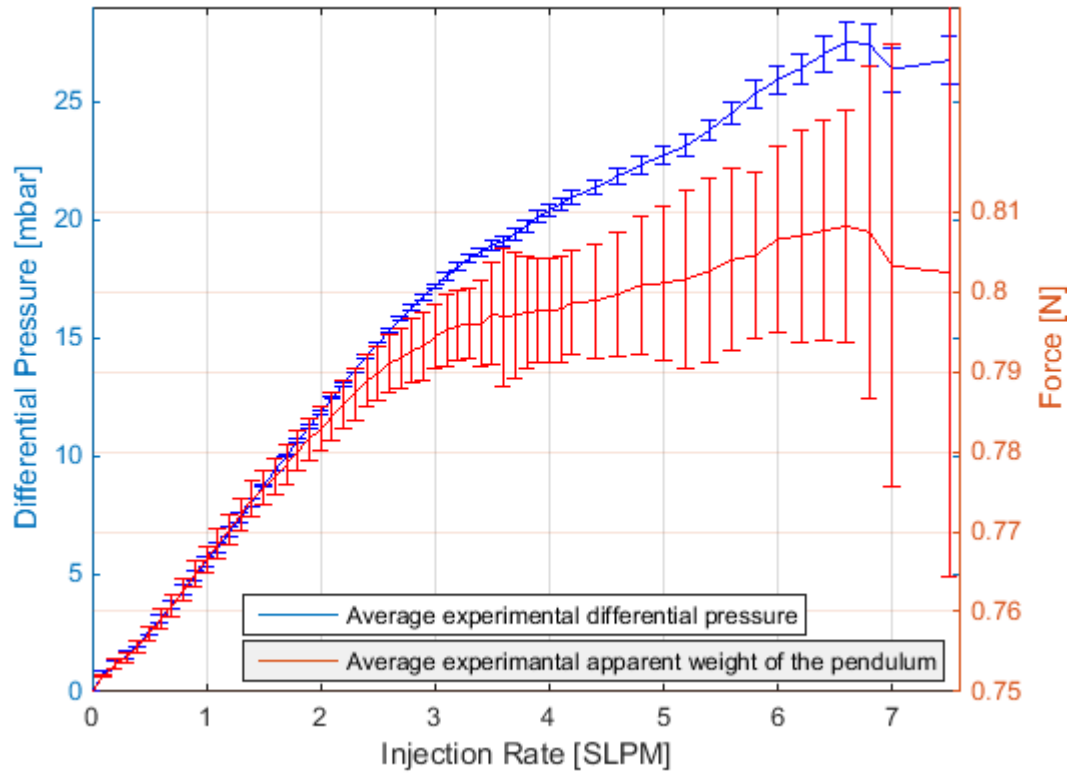


Figure 34 Average experimental apparent weight vs average experimental differential pressures for different gas injections

From Figure 34 we can see that there is a similar trend through the experiment between the apparent weight measured by the force sensor and the differential pressure measured by the differential pressure gauge. Indicating that the apparent weight of the pendulum is highly related to the differential pressure. This result indicates that the apparent weight of the pendulum is highly related to the pressure gradients. This was expected since the buoyancy is related to change in pressure. The differential pressure graph seems steeper than the average change in the force curve. To investigate this further, the differential pressure is calculated into the change in buoyant force of the pendulum(bob). This was found by using the differential pressure Equation 4.5 and the buoyancy Equation 2.2. The buoyancy of the bob by using Equation 2.2 can be written as:

$$F_B = (P_{\text{bot}} - P_{\text{top}})_{\text{bob}} A_{\text{bob}} \quad \text{Equation 5.3}$$

While Equation 4.5 can be written as:

$$\Delta p_{\text{riser}} = \rho_w g \Delta h - p_{\text{diff}} \quad \text{Equation 5.4}$$

Where the Δp_{riser} in Equation 5.4 is the difference in pressure between the pressure at pressure tap 1 and pressure tap 2 in the riser, which makes $\Delta p_{\text{riser}} = (P_{\text{bot}} - P_{\text{top}})_{\text{pressure taps}}$.

Which gives:

$$(P_{\text{bot}} - P_{\text{top}})_{\text{pressure taps}} = \rho_w g \Delta h - p_{\text{diff}} \quad \text{Equation 5.5}$$

Since the bob is placed between the two pressure taps, the difference in pressure between the top and bottom of the bob $((P_{\text{bot}} - P_{\text{top}})_{\text{bob}})$ can be estimated by correction for the difference in height:

$$(P_{\text{bot}} - P_{\text{top}})_{\text{bob}} = \frac{h_{\text{bob}}}{\Delta h} (P_{\text{bot}} - P_{\text{top}})_{\text{pressure taps}} \quad \text{Equation 5.6}$$

Which gives the the relation between the difference in pressure between the top and bottom of the bob and the differential pressure measured:

$$(P_{\text{bot}} - P_{\text{top}})_{\text{bob}} = \frac{h_{\text{bob}}}{\Delta h} (\rho_w g \Delta h - p_{\text{diff}}) \quad \text{Equation 5.7}$$

By inserting Equation 5.7 into Equation 5.3 the relation between the buoyancy of the bob and differential pressure then becomes:

$$F_B = \frac{h_{\text{bob}}}{\Delta h} (\rho_w g \Delta h - p_{\text{diff}}) A_{\text{bob}} \quad \text{Equation 5.8}$$

By using Equation 2.8 the change in apparent weight of the pendulum if only considering buoyant forces is given by:

$$\Delta W'_B = (F_g - F_{B,m}) - (F_g - F_{B,w}) = F_{B,w} - F_{B,m} \quad \text{Equation 5.9}$$

When the pipe is filled with water the differential pressure is equal to zero. By inserting Equation 5.8 into Equation 5.9 the apparent weight of the pendulum if only considering buoyant forces becomes:

$$\Delta W'_B = \frac{h_{\text{bob}}}{\Delta h} (\rho_w g \Delta h) A_{\text{bob}} - \frac{h_{\text{bob}}}{\Delta h} (\rho_w g \Delta h - p_{\text{diff}}) A_{\text{bob}} \quad \text{Equation 5.10}$$

Which gives the relation between the differential pressure measured by the pressure gauge and the change in apparent weight of the pendulum due to buoyant forces:

$$\Delta W'_B = \frac{h_{bob}}{\Delta h} P_{diff} A_{bob} \quad \text{Equation 5.11}$$

The distance between the two pressure taps, Δh , and the height of the bob, h_{bob} can be found in Chapter Flow loop with pressure gauges 3.2.1 and Chapter 5.1.2.2. Due to the shape of the bob the areal is not always constant. An average areal was found by dividing the volume of the bob with the height of the bob The volume of the bob, can be found in Chapter 5.1.2.2.

$$A_{bob} = \frac{V_{bob}}{h_{bob}} = \frac{30.0 \text{ cm}^3}{85 \text{ cm}} = 0.353 \text{ cm}^2 \quad \text{Equation 5.12}$$

By inserting the values for height of the bob, the distance between the two pressure taps and the relation between the differential pressure measured by the pressure gauge and the change in apparent weight of the pendulum due to buoyant force becomes:

$$\Delta W'_B = \frac{h_{bob}}{\Delta h} P_{diff} A = \frac{0.85 \text{ m}}{1 \text{ m}} P_{diff} \cdot 10^2 \frac{\text{Pa}}{\text{mbar}} 0.353 \text{ cm}^2 * 10^{-4} \frac{\text{m}^2}{\text{cm}^2} \quad \text{Equation 5.13}$$

Which gives the relation between change in apparent weight of the pendulum due to buoyant force and the differential pressure:

$$\Delta W'_B = 0.003 P_{diff} \quad \text{Equation 5.14}$$

By using Equation 5.14 to convert the average differential pressure curve in Figure 28 into change apparent weight due to the buoyant force, the blue curve “Expected change in apparent weight due to buoyant forces” in Figure 35 is created. The red curve is the change in average experimental apparent weight of the pendulum from Figure 27. The yellow curve in Figure 27 present the difference in force between the average experimental change in apparent weight of the pendulum and the expected change in apparent weight due to buoyant forces acting on the pendulum.

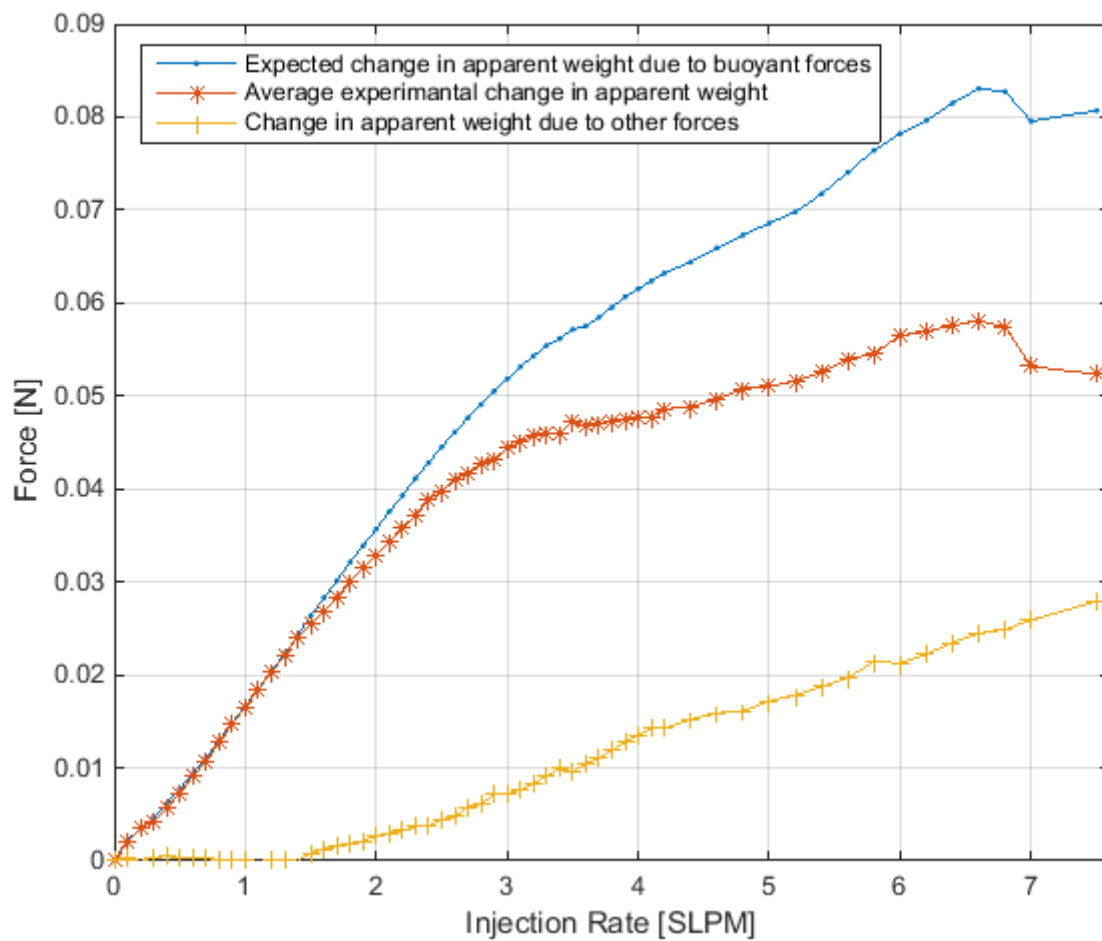


Figure 35 forces affecting the apparent weight of the pendulum (experiment 1)

From Figure 35 shows that the average change in apparent weight of the pendulum measured from the experiments only depends on the buoyant force up to an injection rate of 1.4 SLPM. Which is the same conclusion from the comparison between Archimedes principle and the apparent weight of the pendulum in Figure 33. Remember, Archimedes principle does only account for changes in the hydrostatic pressure gradient and does not account for changes due to the frictional pressure gradient. By using the differential pressure data from the experiments to the frictional pressure gradient is included in the buoyant force. After an injection rate of 1.4 SLPM the comparison in Figure 35 shows that the result of the average apparent force of the pendulum depends on a buoyant force and a force which is increasing almost linearly with the increase of the injection rate. This force is most likely caused by viscous forces. In Chapter 5.1.2.2 it was mentioned that drag forces contribute to decrease the apparent weight of the pendulum. Drag forces as can be seen from Equation 5.1 will increase as the velocity increase.

The linear increasing force may therefore be connected to a drag force. Similar result from experiment 2 and 3 can be found in the Appendix.

Figure 36 shows an indication of the different forces that affects the apparent weight of the pendulum. The figure shows the average apparent weight as a function of gas injections rates (Figure 27) with numbers and color codes representing different forces that affects the apparent weight. An explanation of the figure is given below.

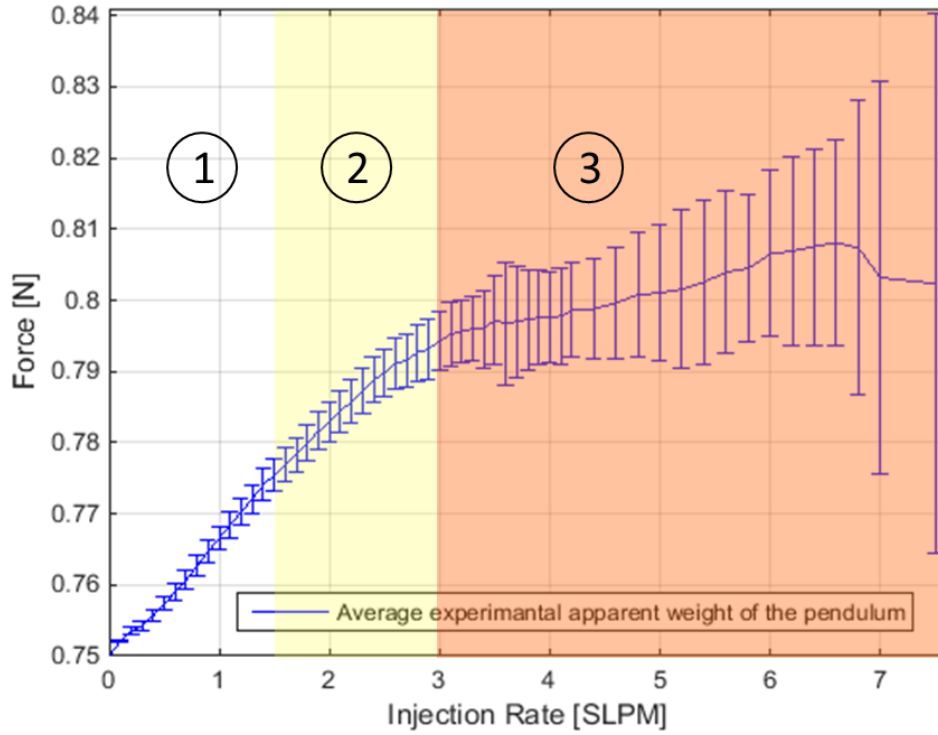


Figure 36 Different forces that affects the apparent weight of the pendulum

The number and color codes in Figure 36 :

1. The white zone indicates that up to a gas injection rate of 1.4 SLPM the apparent force of the pendulum is only affected by the gravitational force and the hydrostatic pressure gradient. This was concluded from the analysis of Figure 33. Here the Archimedes principle is applicable and the gas fraction can be calculated from the average apparent force of the pendulum by solving Equation 4.29 for gas fraction:

$$\varepsilon_g = \frac{W' - F_g + \rho_w g V_{\text{bob}}}{g V_{\text{bob}} (\rho_w - \rho_g)} \quad \text{Equation 5.15}$$

Where ε_g is gas fraction, W' is the average apparent force of the pendulum measured by the force sensor, F_g is true weight of the pendulum, ρ_g and ρ_w is the density of gas and water, respectively and V_{bob} is the volume of the bob.

2. In the yellow zone a force increasing linear with the injection rate starts to decrease the apparent weight of the pendulum. This linear force was found in Figure 35 by comparing the difference in force between the average experimental change in apparent weight of the pendulum and the expected change in apparent weight due to buoyant forces acting on the pendulum. The linear force is believed connected to viscous forces.
3. In the orange zone the frictional pressure drop start to affect the apparent weight of the pendulum. In the analysis of *Figure 30* it was found that frictional gradients started to affect the pressure when the gas injection rate was higher than 3 SLPM. Since the apparent weight is effected by the buoyancy, which is effected by the pressure, the frictional pressure drop will affect the apparent weight of the pendulum.

From the analysis this section, it may be concluded that even though the gas fraction measured from the apparent weight and the differential pressure method seems to be two completely different methods of finding the gas fraction in a pipe, they are based on the same theory. Both methods calculate the gas fraction based on changes in pressure gradients. Apart from that the apparent weight is also effected by a force that grows with increasing gas injection rate. Which is believed to be caused by viscous forces.

5.2.6.2 Alternative method to determine the gas fraction from a buoyancy Sensor

This section will contain an alternative method to determine the gas fraction in the pipe, by using a frequency spectrum analysis. This method will only be presented as an alternative idea for future studies, and will not be analyzed.

A frequency spectrum analysis creates a frequency spectrum from a time series $f(t)$ by using the Fourier transform[2]. When the apparent weight is oscillating a single wave will appear as a peak in the frequency spectrum analysis where the y-axis represent the amplitude and the x-axis represent the Frequency of the wave. A strongly flocculating apparent weight will be characterized by broad spectrum where many frequencies appear. Figure 37 shows two examples of a single sided frequency spectrum analysis. To the left is a frequency spectrum analysis when the gas injection rate is 0.2. The frequency spectrum analysis to the right is for

an injection rate of 7.4 SLPM. The frequency spectrum analysis may be used to recognize different frequency spectrums for different gas fractions. The idea is that each injection rate/gas fraction will have its own recognizable frequency spectrum pattern.

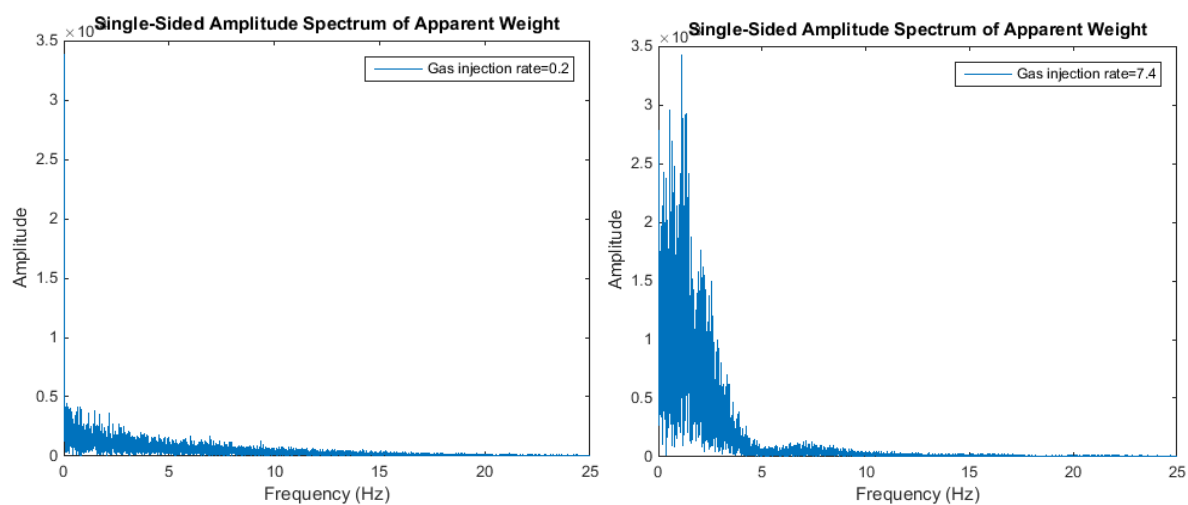


Figure 37 FFT analysis for left) 0.2 SLPM right) 7.4 SLPM

The MATLAB code for this analysis is given in the Appendix.

6. Conclusion

A wide variety of methods for measuring in-situ gas fraction in gas-liquid flows exist, based on different principles. However, there is still a need for new methods to measure the fractions in exact, fast and simple ways. The new method presented in this thesis has a simple setup, and measures the fractions through the use of a buoyance sensor.

To test if it is possible to measure gas fractions this way, experiments have been carried out at the Multiphase Laboratory at University of Stavanger. These experiments required the development of an experimental setup and a new test methodology. Different equipment and different experimental conditions were tried out before an adequate experimental setup and way of running the experiments were developed.

The method developed exploits relevant theory, and is based on using a force sensor to measure the apparent weight of an ideally stationary object. The object is attached to the force sensor like a pendulum, and immersed in a fluid filled pipe. The gas fractions inside the tube is controlled by injecting gas from the bottom of the pipe.

To verify the results that this method produced in a laboratory setting, the results were compared with the in-situ gas fractions calculated by the use of two other existing methods for measuring gas fractions. Readings of the liquid level of fluid inside the pipe and measuring by the use of a differential pressure gauge were done simultaneously, and integrated in the experimental setup.

Based on the experimental work and analysis some main conclusions can be drawn:

- The experimental results are highly dependent on the design and density of the pendulum, the viscosity of the fluid and the dispersion of gas bubbles, which may indicate that the apparent weight is highly affected by viscous forces. Due to this the most adequate pendulum was found to have a small diameter.
- Using Archimedes principle to find gas fraction in a gas-liquid flow is applicable if friction pressure drop and what is believed to be viscous forces are negligible.
- The results from the experiments showed a clear connection between the apparent weight of the pendulum measured by the force sensor and the expected change in apparent weight due to buoyant forces for different injection rates. However, when gas injections increased above a certain level, other forces started to affect the apparent weight.

- The apparent weight of the pendulum is affected by hydrostatic pressure drop, frictional pressure drop and a force which appear to grow linear with increased gas injection.
- Even though the gas fraction measured from the apparent weight and the differential pressure method seems to be two completely different methods of finding the gas fraction in a pipe, they are based on the same theory. Both methods calculate the gas fraction based on changes in pressure gradients. Apart from that the apparent weight is also affected by a force that grows with increasing gas injection rate. Which is believed to be caused by viscous forces.

Summing up, the results of the research are an adequate new laboratory setup and a new experimental methodology for this kind of research. A new method for measuring gas fractions in gas lift flow has been developed and tried out with encouraging results. However, a way of identifying and controlling for unknown forces that affect the results needs to be developed, if the method shall have any future. Furthermore, other weaknesses are that the research is based on small scale testing in a laboratory, the test variables have been limited, the experiments few and have been carried out under controlled conditions. Based on the learning and experiences done in this thesis, some ideas for further research and future studies are presented in the next chapter.

7. Future studies

The experiments carried out in this study, shows that gas fractions may be measured with a buoyance sensor when the gas injection rates are low and under certain experimental conditions. The results from the experiments are promising, but further research and development are required before any conclusions can be made. Based on the practical experiences, the theoretical discussions and the identified uncertainties and weaknesses described in the previous chapters, some suggestions for future studies are presented below.

1. Study, identify and control for the unknown linearly increasing force that affect the apparent weight of the submerged pendulum through more experiments
 - Find the origin of the unknown force
 - Increase the range of gas injection rate. Will the force still grow linearly or will this change?
 - Change the areal of the bob and identify the pattern of effect of the unknown force
 - Integrate the pattern of effect of the unknown forces in the methodology to ensure exact and reliable measurements
2. If the results from 1) are successful, run the experiments at a larger scale
3. If the results from 2) are successful, develop a full scale test facility that can be tried out in a real industrial setting

An other suggestion for finding gas fraction was suggested in Chapter 5.2.6.2. Where a frequency spectrum analysis may be used to recognize different frequency spectrums for different gas fractions.

References (EndNote)

1. John W. Jewett, J.R.A.S., *Physics for Scientists and Engineers* ed. t. edition. Vol. 1. 2010.
2. Time, R.W., *Two-Phase Flow in Pipelines - course compendium*. 2009, University of Stavanger.
3. Taitel, Y., D. Bornea, and A. Dukler, *Modelling flow pattern transitions for steady upward gas-liquid flow in vertical tubes*. AIChE Journal, 1980. **26**(3): p. 345-354.
4. Tor David Østvold, E.M., *Optimization of Gas Lift Flow Loop, in Petroleum Technology*. 2014, University of stavanger: Stavanger.
5. *Personal communication with Rune W. Time*. 2017.
6. Jia, J., A. Babatunde, and M. Wang, *Void fraction measurement of gas-liquid two-phase flow from differential pressure*. Flow Measurement and Instrumentation, 2015. **41**: p. 75-80.
7. Robert, B., *New experiments physico-mechanical, touching the spring of the air, and its effects (Made, for the most part, in a New Pneumatical Engine)*. 1973.
8. Gazizzullin, E., *Gas lift simulation and experiments in conjunction with the lyapkov P.D methodic, in Petroleum Engineering*. 2016, University of stavanger: Stavanger.
9. Clark, R. and K. Bickham. *A mechanistic model for cuttings transport*. in *SPE Annual Technical Conference and Exhibition*. 1994. Society of Petroleum Engineers.
10. Eigeldinger, J. and H. Vogt, *The bubble coverage of gas-evolving electrodes in a flowing electrolyte*. Electrochimica Acta, 2000. **45**(27): p. 4449-4456.
11. PASCO. Available from: <https://www.pasco.com/prodCompare/force-sensors/index.cfm>.
12. Mark-10. Available from: <http://www.mark-10.com/instruments/indicators/Si.html>.

Appendices

A. Specifications

A.1 PASCO Measurement Equipment

PASCO 5N Load Cell PS-2201

	Force [N]
Range	± 5
Accuracy	± 0.05
Resolution	0.001
Overload without damage	± 7.5

wired with a male 6-pin mini-DIN connector for plugging into a PASCO Load Cell Amplifier which is connected to the computer through a PASCO 850 universal interface



Figure 38 a PASCO 850 universal interface, 6-pin mini-DIN connector and PASCO 5N Load Cell PS-2201

Source for PASCO equipment: [11]

A.2 Mark-10 Measurement Equipment

Mark-10 MR03-05 Force Sensor

	Force [N]
Range	± 2.5
Accuracy	$\pm 0.15\%$ of full scale (± 0.00375)
Resolution	0.001

Connected to the computer through the Mark-10 M50 indicator

Connectivity:

Mark-10 M5i Indicator

	Force [N]
Accuracy	$\pm 0.1\%$ of full scale (0.0025)
Resolution	0.0005
Safe Overload	150% of full scale

Max sample rate: 7000 Hz

Connectivity: Automatic data output via UBS/RS-232



Figure 39 Mark-10 M5i indicator and a R03-05 force sensor

Source for Mark-10 equipment: [12]

A.3 Alicat flow meter

Alicat Scientific, Inc.
7641 N. Business Park Dr., Tucson, AZ 85743 U.S.A., 1.888.290.6060
Calibration Data Sheet
Certification Number: 127680

Customer: Kompauto Nordic AB
Sales Order Number: SO325465
Serial Number: 122780
Model Number: MCR-50SLPM-D
Customer Part Number: KA1300001537
Software Version: 5v12.0-R22
P/D/I Values: 100 / 15000 / 0
Adder Codes: 5M, 5IN, GAS: Air
Process Gas: Selectable
Calibration Gas: Air
Range: 50.00 SLPM
Gas Temperature: 22.4°C
Ambient Humidity: 47%
Calibration Procedure/Rev. #: DOC-AUTOCAL-GASFLOW/Rev. 87
Calibrated By: Pablo De La Cruz
Calibration Date: 10/9/2015
Full Scale Pressure: 160.00 PSIA
Full Scale Pressure Accuracy: $\pm 0.5\%$ of Full Scale
Temperature Accuracy: $\pm 1.5^\circ\text{C}$
Standard Temp. & Pressure: 25°C, 14.6959 PSIA
Calibration due 1 yr. after receipt:

Equipment Used

Flow: TOOL-FLOW13	Temperature: TOOL-TEMP18
Tool Due Date: 1/3/2016	Tool Due Date: 6/14/2016
Manufacturer/Model: Alicat / MCM-50SLPM-D	Manufacturer/Model: SELCO
Device Uncertainty: $\pm 0.3\%$ Reading + 0.2% F.S.)	Device Uncertainty: $\pm 0.75^\circ\text{C}$
Pressure: TOOL-PRESSURE8	Volume: TOOL-VOLUME14
Tool Due Date: 3/9/2016	Tool Due Date: 1/15/2016
Manufacturer/Model: Alicat / P-100PSIG-D	Manufacturer/Model: Fluke 87-5
Device Uncertainty: $\pm 0.2\%$ of full scale	Device Uncertainty: $\pm 0.1\% + 1$ digit)

All test equipment used for calibration is NIST traceable.

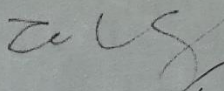
Calibration

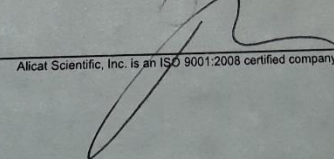
Uncertainty: $\pm 0.8\%$ of Reading + 0.2% of Full Scale) Calibration Pressure: Inlet: 50 PSIG
Units of measure: SLPM Outlet: 0 PSIG

Output 1 Configuration mini-DIN Pin #6	Output 2 Configuration mini-DIN Pin #2
--	--

D.U.T.	Actual	In Tolerance	Output 1	Output 2
0.00	0.00	Yes	0.000 Vdc	5.12 Vdc
12.48	12.47	Yes	1.248 Vdc	5.12 Vdc
24.99	24.98	Yes	2.499 Vdc	5.12 Vdc
37.53	37.50	Yes	3.750 Vdc	5.12 Vdc
49.98	50.06	Yes	5.00 Vdc	5.12 Vdc

Notes: 0-5V set-point.

Tech Signature: 

QC Signature: 

Alicat Scientific, Inc. is an ISO 9001:2008 certified company. CS1 Rev 16 Last Modified 01/18/2013

Figure 40 Alicat Flow meter calibration data sheet

B. MATLAB

```
%% Reading the experimental data from the Feasibility
experiment

clc;
close all;
clear;

A = xlsread('exp20423');      %excel sheet for experiment

% no inj
inj_deg=8
h_w=47.7;      %Liquid level of water
inj_s=10;      %Time start
inj_e=60; %time end
eg=0          % gas fraction

% injection 1
% h_m= 47.9      ; %Liquid level of mixture fluid
% inj_s= 240      ;
% inj_e= 320      ;
% eg=(h_m-h_w)/h_m; %gas fraction, liquid level method

% % injection 2
% inj_deg= 8
% h_m= 48.4      ;
% inj_s=380      ;
% inj_e= 500      ; %
% eg=(h_m-h_w)/h_m; %liquid level method

Time_vector=A(:,2);

Start_t = inj_s;      %Time experiment starts
tmp = abs(Time_vector-Start_t);
[idx idx] = min(tmp);      %index of closest value
ts = Time_vector(idx);      %closest value
a=find(ts==A(:,2));

end_t = inj_e;      %Time experiment starts
tmp = abs(Time_vector-end_t);
[idx idx] = min(tmp);      %index of closest value
te = Time_vector(idx);      %closest value
b=find(te==A(:,2));

Time=A(a:b,2);
```

```

Force=(-1)*(A(a:b,1)); %Apparent weight vector
average=mean(Force) %Findig average value
stand_div = std(Force) %standard deviation

```

Apparent weight (force), standard deviations (SD), gas fractions (eg) and injection rate are transferred to a separate excel worksheet

```

%% Reading the experimental data from the main experiments

```

```

clc;
close all;
clear;

```

```

Exp='Experiment';
nr=1;

```

```

%% Mark-10
A = xlsread('exp10608'); %excel sheet for experiment
with force data given by Mark-10

```

```

%% Labview
B = xlsread('lab0608'); %excel sheet for experiment
with gas flow, pressure and temperature data from Labview

```

```

start_lab= 42.34 ; % Time lag in LabVIEW

```

```

%%
P_b=302; %Bottom hole pressure
dT=400; %time [s] elapsed between
changing injection rate (dinj)
Sa=50; %safety time [s] value to
make shore that the injection rate has been
changed/stabilized
St_inj=0.2; %Start injection rate
[SLPM]
dinj=0.2; %Change in injection rate
[SLPM]
% D_tube=3.93; %inner diameter of tube

```

```

for n=(1:28) %(1:28) Number of steps
    injection_number=n;
    A_injection_number(n)=injection_number;

```

```

%finding time an injection rate in each step
inj_s= (dT*(n-1))+Sa ; %Time when the
injection of a specific injection rate, i, starts [s]

```

```

inj_e= (dT*(n))-Sa ; %Time when the injection of
a specific injection rate, i, ends [s]
inj_rate=St_inj+(dinj*(n-1)); %Injection rate i
[SLPM]
inj_rates(n)=inj_rate; %all injection rates

%% Labview

Time_Lab=B(:,1); %Time vector
in the Labview excel worksheet
%rownumberlast (for time..

%find the "step" ...fix

Start_t_lab = (inj_s)+start_lab; %Time experiment
starts
tmp_lab = abs(Time_Lab-Start_t_lab);
[idx idx] = min(tmp_lab); %index of closest
value
ts_lab = Time_Lab(idx); %closest value of
injection end time (inj_s) that are
recorded by Labview in the excel worksheet
a_lab=find(ts_lab==B(:,1)); %step in excel worksheet
where ts_lab are recorded

end_t_lab = (inj_e)+start_lab; %Time
experiment starts
tmp_lab = abs(Time_Lab-end_t_lab);
[idx idx] = min(tmp_lab); %index of closest value
te_lab = Time_Lab(idx); %closest value of injection
end time (inj_e) that are recorded
by Labview in the excel woorksheet
b_lab=find(te_lab==B(:,1)); %step in excel worksheet
where te_lab are recorded

%Time_inj_lab=B(a_lab:b_lab,1); %all times were the injection
rate = i , in the Labview excel worksheet

%% Analyzing the data from Labview

%using the Relative differential pressure to find the gas
fraction in injection i
Rel_Diff_press=(B(a_lab:b_lab,2)); %Relative
differential pressures read from the
Labview excel worksheet for
injection i
Rel_Diff_press_average=mean(Rel_Diff_press);
A_Rel_Diff_press(n)=Rel_Diff_press_average;% average Relative
differential pressure

```



```

SD_Rel_Diff_press=std(Rel_Diff_press);
A_SD_Rel_Diff(n)=SD_Rel_Diff_press;
ro_w=1000; %Density
of water
ro_g=1.3 ; %STD
Density of gas
g=9.81;
%gravitational constant [m/s]
eg_cal=((100*Rel_Diff_press)/((ro_w-ro_g)*g)); %gas fractions
calculated from the differential pressure
eg=mean(eg_cal);
A_eg(n)=eg;
eg_SD= std(eg_cal);
A_eg_SD(n)=eg_SD;

A_Gas_fractions(n)=eg;
inj_rate=(B(a_lab:b_lab,7));
inj_rate_SLPM=mean(inj_rate);
%injection flow rate i actually injected [LPM]
A_inj_rate_SLPM(n)=inj_rate_SLPM;
gas_flow=(B(a_lab:b_lab,8));
gas_flow_SLPM=mean(gas_flow);
%injection flow rate flowing in SLPM
A_gas_flow_SLPM(n)=gas_flow_SLPM;
gas_flow_lab=(B(a_lab:b_lab,4));
gas_flow_LPM=mean(gas_flow_lab) ;
%injection flow rate i actually injected [LPM]
A_gas_flow_LPM(n)=gas_flow_LPM;

h0_lab=100*P_b/(ro_w*g); % waterhight
calculated by the bottomhole pressure
A_h0_lab(n)=h0_lab;

%% Data From Mark-10 excel sheet

%corecting for matlab aquistition frequency error to find the
... where
%where

Time_vector=A(:,3); % all time recorded by Mark-10
during the experiment

tmp = abs(Time_vector-inj_s);
[idx idx] = min(tmp); %index of closest value
ts = Time_vector(idx); %closest value of
injection start time (inj_s) that are recorded by mark-10 in
the excel worksheet
a=find(ts==A(:,3)); %steps in excel
worksheet where ts are recorded

```

```

tmp = abs(Time_vector-inj_e);
[idx idx] = min(tmp);           %index of closest value
te = Time_vector(idx);          %closest value of injection
end time (inj_e) that are recorded by mark-10 in the excel
worksheet
b=find(te==A(:,3));             %steps in excel worksheet
where te are recorded

Time=A(a:b,3);                  %all times were the injection
rate = i , in the Mark-10 excel worksheet

Force=((-1)*(A(a:b,2))); %Apparent weight vector for
injection rate i

%%
%Findig average value

Fmean=mean(Force);

stand_div = std(Force);
A_SD(n)=stand_div;              %all
F_ave
%standard deviation
%
Highest=max(Force);             %Highest force value measured
for injection i
Lowest=min(Force);              %lowest force
value measured for injection i
All the parameters used for plots was transferred to an new
excel sheet

%% FFT Analysis

%corecting for matlab acquisition frequency error
Tmax = max(Time);
dt=0.02;
Tmin = min(Time);
Tsnew = Tmin:dt:Tmax;          % Sampling period (for this injecti)
Finterp1 = interp1(Time,Force,Tsnew);

%
Fs = 1/dt;
L=length(Tsnew);               % Length of signal ( amount of test data
used in this analysis)
NFFT = 2^nextpow2(L); % Next power of 2 from length of y
Uintermean=(Finterp1-Fmean); % removing the average value to
better see the other peaks in the FFT analysis
Y = fft(Uintermean,NFFT)/L;

```

```

f = Fs/2*linspace(0,1,NFFT/2);

figure(400+n)
% Plot single-sided amplitude spectrum.
plot(f,2*abs(Y(1:NFFT/2)))
hold on
title('Single-Sided Amplitude Spectrum of Apparent Weight')
xlabel('Frequency (Hz)')
ylabel('Amplitude')
legend(strcat('Gas injection rate=', num2str(inj_rate_SLPM)))
% legend(eg)

Fs = 1/dt; % Sampling frequency
L=length(Tsnew);
NFFT = 2^nextpow2(L); % Next power of 2 from length of y
Uintermean=smooth(Finterp1-Fmean);
Y = fft(Uintermean,NFFT)/L;
f = Fs/2*linspace(0,1,NFFT/2);

figure(500+n)
% Plot single-sided amplitude spectrum.
plot(f,2*abs(Y(1:NFFT/2)))
hold on
legend(strcat('Gas injection rate=', num2str(inj_rate_SLPM)))
title('smooth Single-Sided Amplitude Spectrum of Apparent
Weight')
xlabel('Frequency (Hz)')
ylabel('Amplitude')

```


C. Figures



Figure 41 The Feasibility setup with the PASCO 5N Load Cell PS-2201



Figure 42 Sowing thread sticking to the pipe

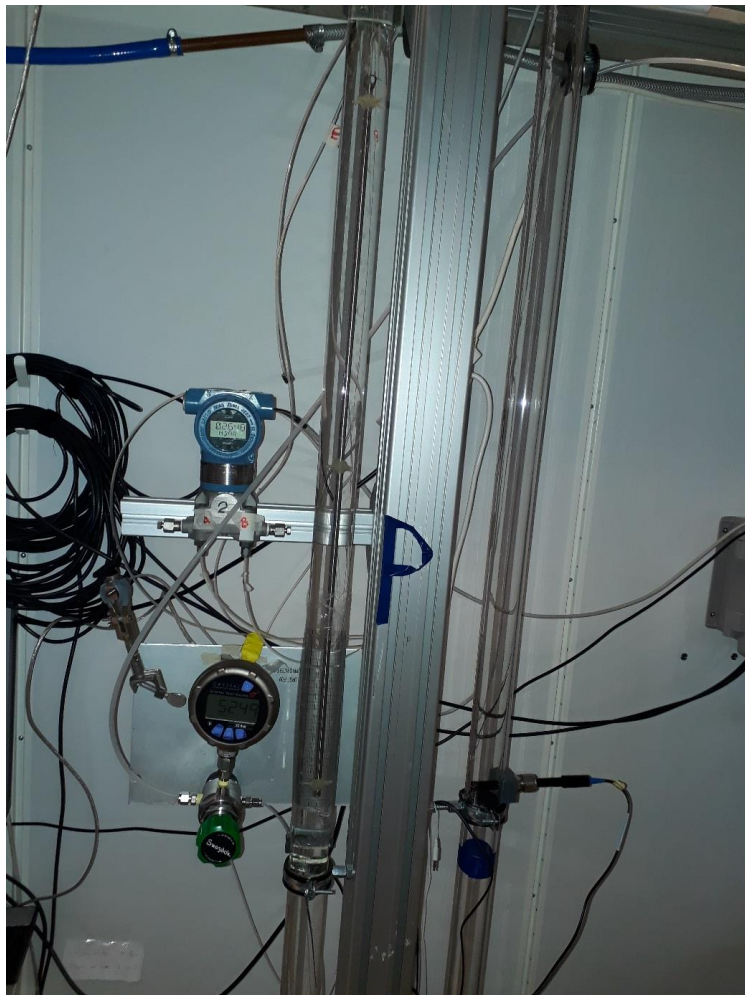


Figure 43 The steel bar inside the flow loop

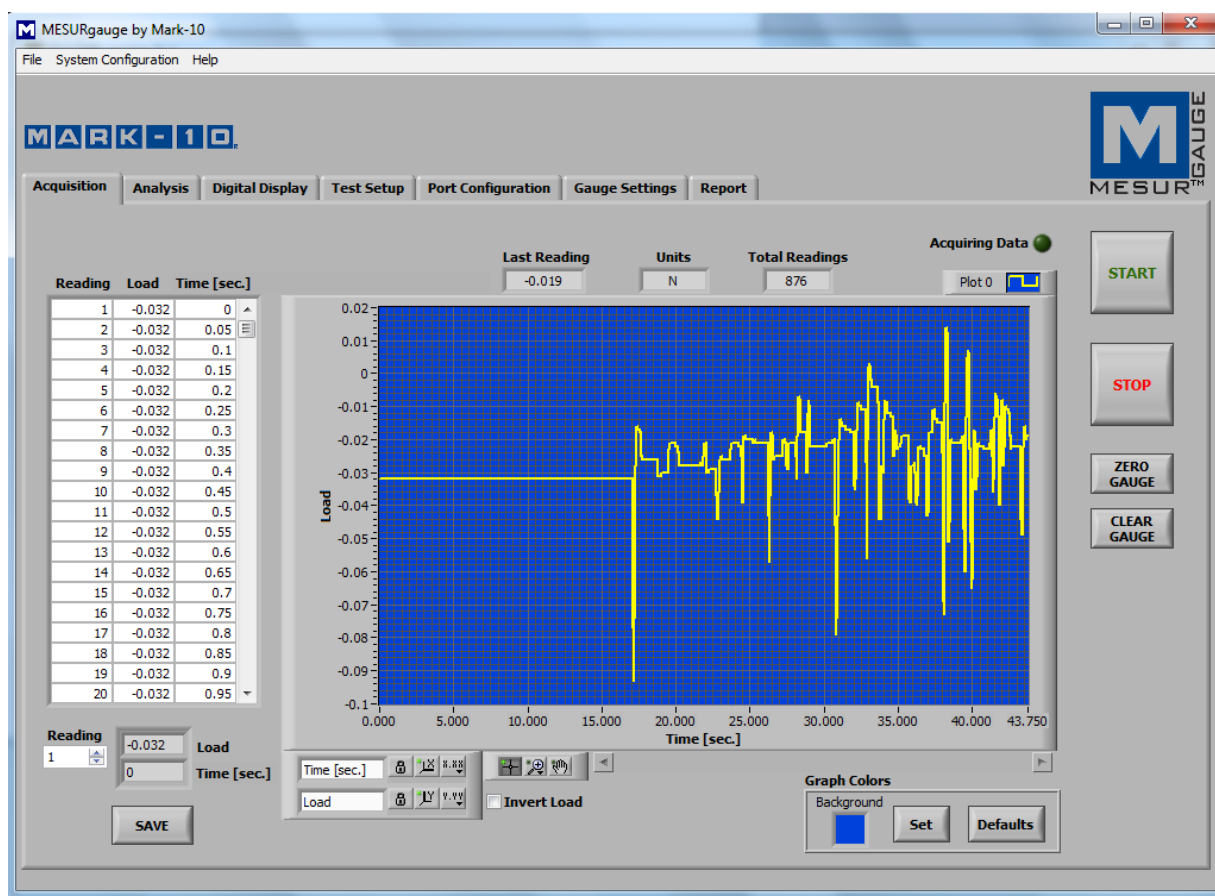


Figure 44 Mark-10 front panel

Calibration of the Differential Pressure Gauge

From the calibration of the pressure gauge described in chapter 3.3.3 the standard deviations of the differential pressure was reduced as shown in *Figure 46*. Where the standard deviations of the differential pressure is a function of gas fraction.

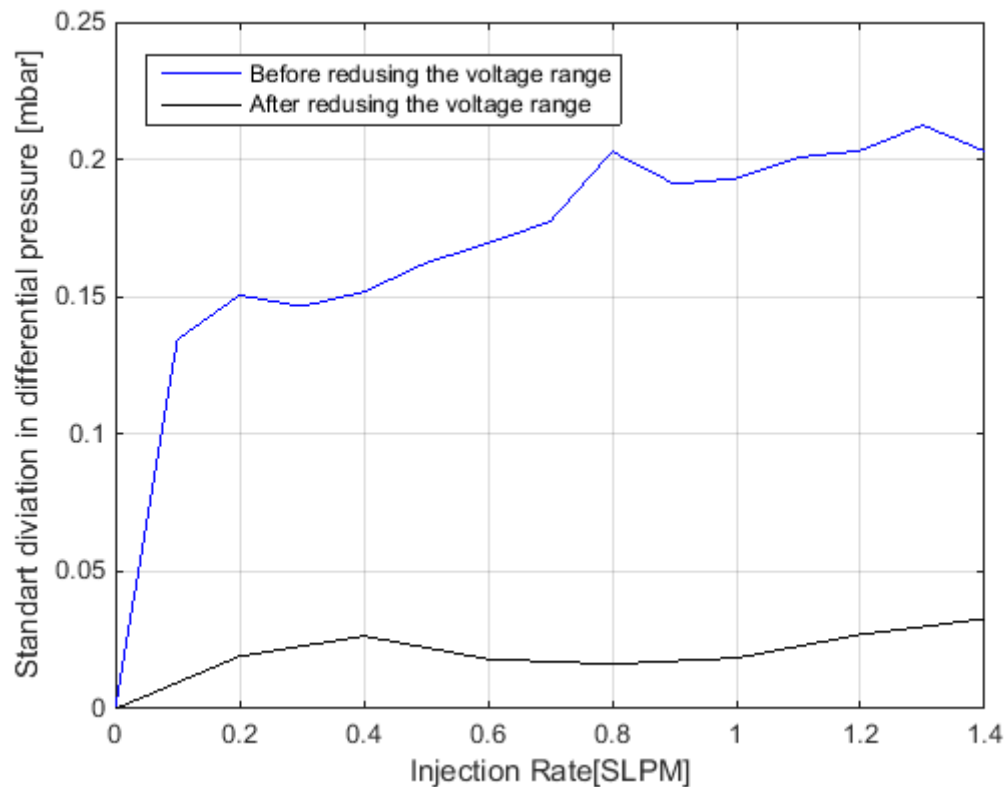


Figure 46 Reduction in error from calibration of the differential pressure gauge

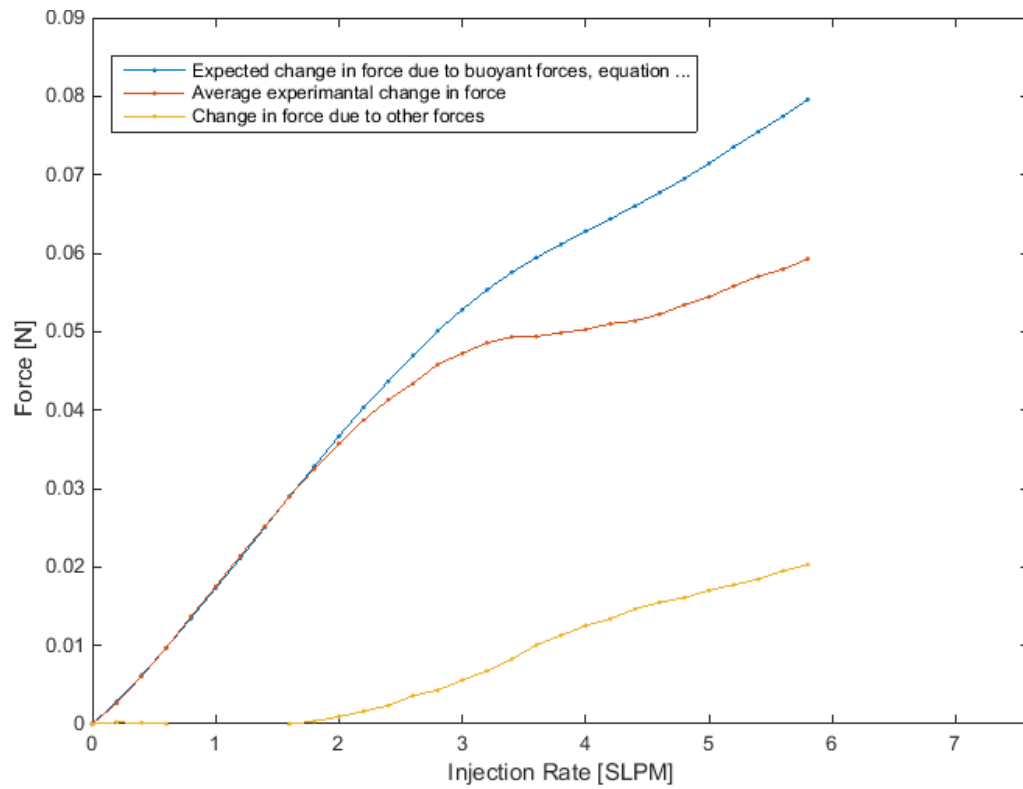


Figure 47 forces affecting the apparent weight of the pendulum (experiment 2)

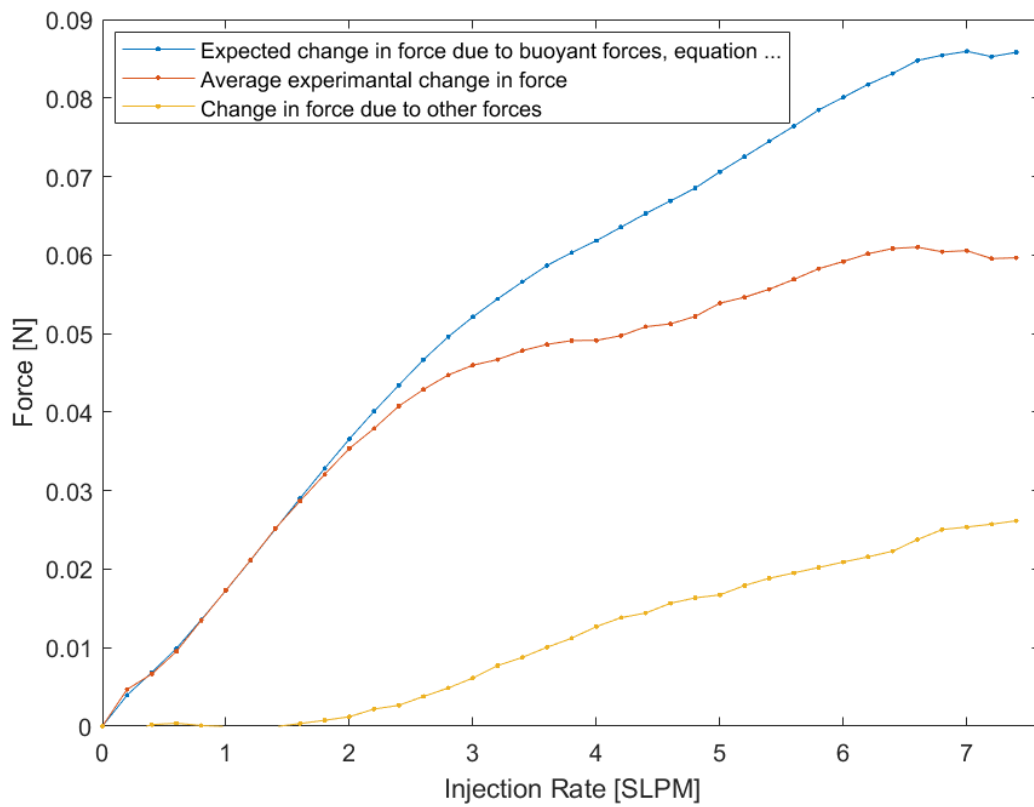


Figure 48 forces affecting the apparent weight of the pendulum (experiment 3)

Nomenclature

Abbreviations

SLPM: Standard liter per minute

Greek letters

β	Inclination
ε_g	Gas fraction
$\overline{\varepsilon_g}$	Average gas fraction
ε_L	Liquid fraction
Δh	Height between pressure tap 1 and 2 [m]
Δp	Pressure drop between pressure tap 1 and 2 [m]
Δp_f	Frictional pressure drop between pressure tap 1 and 2 [m]
θ	degree
μ	Viscosity [Pas]
μ_m	Fluid mixture viscosity [Pas]
ρ	Density [kg/m ³]
ρ_g	Gas density [kg/m ³]
ρ_L	Liquid density [kg/m ³]
ρ_m	Fluid mixture density [kg/m ³]
ρ_{bob}	Bob density [kg/m ³]

Roman Letters

A	Areal [m ²]
A _{bob}	Areal of bob [m ²]
A _{tube}	Areal inside the tube [m ²]
D	diameter [m]
F _B	buoyancy [N]
F _g	Gravity force [N]
F _d	drag force [N]
g	Acceleration due to gravity [m/s ²]
h	Height [m]
h _{bob}	height of bob [m]

h_{bot}	Height at bottom [m]
h_{fluid}	Height of mixed fluid [m]
h_{top}	Height at top [m]
h_w	Height of water in tube [m] [cm]
L	Length [m]
m	Mass [kg]
P	Pressure [Pa]
P_0	Reference pressure
P_1	Pressure tap 1
P_2	Pressure tap 2
P_{atm}	Atmospheric pressure [Pa]
P_{bot}	bottom pressure [Pa]
P_{top}	top pressure [Pa]
p_{diff}	Differential pressure [mbar]
$\overline{p_{\text{diff}}}$	Average differential pressure [mbar]
U_{GS}	Superficial gas velocity [m/s]
U_{LS}	Superficial liquid velocity [m/s]
V	Volume [m^3]
V'	Volume ratio [m^3/m^3]
V_{bob}	Volume of the bob [m^3]
V_{disp}	Displaced volume [m^3]
V_m	volume mixed fluid [m^3]
V_g	volume gas [m^3]
V_w	volume water [m^3]
W'	Apparent weight [N]
$\left(\frac{dp}{dx}\right)$	Pressure gradient [Pa/m]
$\left(\frac{dp}{dx}\right)_f$	Frictional pressure gradient
$\left(\frac{dp}{dx}\right)_h$	Hydrostatic pressure gradient
$\left(\frac{dp}{dx}\right)_a$	Acceleration pressure gradient